공학박사학위논문

A Study of Microstructures and defects induced by Non-uniform Lithiation in Crystalline Silicon for Li ion Batteries

리튬이온전지 결정질 실리콘 음극의 불균일 리튬화에 의한 미세구조와 결함에 관한 연구

2017 년 08 월

서울대학교 대학원

재료공학부

강 찬 순

Abstract

In recent, Li ion batteries are widely used many applications such as mobile devices, electric vehicles and supporting power supplier in many instruments because of its high power, energy density and light weight. For a long operation time, high capacity materials for cathode and anode are required to improve devices' properties. Silicon is the one of strong candidates due to highest theoretical capacity (~3500mAh/g) among capable materials for anode. A lot of studies for decades about Silicon as an anode, thermodynamic, kinetics, and mechanical behavior of lithiated Silicon has been remaining unresolved.

At First Chapter, the remarkable microstructure called "band-like lithaition structure" developed in lithiated <100> Si is discussed. Through the localized Li insertion experiment, the origin and criteria of band-like lithiation were revealed. Even though Silicon is covalent bonded materials so known as very brittle. However, dislocations can be generated between at least two neighbor Li_xSi phase growth and it is the strong evidence of plastic deformation of crystalline Silicon. As reported papers about the plastic deformation and dislocation generation, loop formation and its mobile, lithiation in Silicon leads the good environment for taking place plastic deformation of Silicon. And with TEM analysis, crystallographic analysis of lithiation bands were undergone.

In Second Chapter, structural anisotropic Li_xSi phase growth in three basal orientation of Silicon was studied. From many experimental researches, <110> directions and {110} planes have become known as a predominant lithiation direction and planes. Various nano structure such as nano-wire, nano pillar and nano particles were used and anisotropic volume expansion and crack generation by volume expansion were clearly suggested. Comparing to those structures with free surface around their body, local area exposed Silicon wafer with patterns were used for our experiment. Conductive metal and insulator Silicon Dioxide film were deposited for localizing Li insertion. Unlike the structure with free surface, in inside Si wafer, Li_xSi phase growth showed isotropic growth rate along the surface. Even though {110} Si wafer were used, lithiation along normal direction ({110}) was not predominant lithiation direction. These were discussed for finding governing factors to determine the growth rate of Li_xSi in various geometrical and other conditions. Also, the effect of surface electric conductivity was dealt and demonstrated for the relation between Li_xSi phase growth rate.

At Third Chapter, we report a direct observation on the crack behavior of lithiated Si wafer. Three different Si wafers with <100>, <110> and <111> axes are investigated, to compare the crack behaviors of different orientation Si wafers. We find that electrochemically induced cracks in each orientated wafer have dissimilar crack behaviors, because the initiations and propagations of cracks are strongly affected by their orientation and strain energy release rate. It is also found that triangular humps and cracks are formed in the (111) wafer, which are discovered for the first time by our study. Considering that volume expansion, cracks, and pulverizations of Si are the main issues for the commercial use of Si for Li ion battery,

this study provides important insight that is relevant to the design of advanced Si anode materials.

Keywords: Lithium ion battery, Lithiated Silicon, Diffusion, Microstructure, Anisotropic phase growth, Crack propagation

Student Number: 2011-20617

Chan Soon Kang

Table of Contents

List of Figures

Figure 2-2. Surface image of band-like lithiation structure. The band-like lithiation structures are always accompanied with surface roughness. This is a strong evidence of plastic deformation of crystalline Si.

Figure 2-3. Low magnification image of the microstructure developed under surface roughened area, (b) Right under the exposed Si circle and (c) Right under the largest roughened area covered with Cr/Cu/SiO2 diffusion barrier. At (b), bands are forming more complicated structures and thickness of LixSi layer at surface is thinner than neighbor regions. Comparably, simple band-like structures are observed right under the expose Si circles and thickness of LixSi layer at surface is much thicker than (b).

Figure 2-4. Si wafer curvature measurement during lithiation at Gu grid and Cu island pattern on <100> Si wafer. Band-like lithiation formation leads the curvature change difference. This means that band-like lithiation releases the stress during lithiation.

Figure 3-1. Schematics of (a) beaker cell for multi-purpose Li ion battery experiment and (b) unit cell of pattern for local Li insertion to crystalline Si.

Figure 3-2. Lithiated patterned <100>, <110> and <111> Si wafer respectively. Lithiated <111> Si wafer showed the largest volume expansion. Lithiated <110> and <100> Si wafer followed magnitude of swelling in order

Figure 3-3. MD simulation results of local lithiation for each basal orientation of crystalline Si at initial step. MD results show a good agreement with experimental results.

Fig. 3-4 Cross-section images of lithiated patterned <110> Si wafer with various lithiation time (a) 6hrs and (b) 12hrs. During lithiation, LixSi phase growth rate shows same rate along all lateral directions.

Figure 3-5. Cross-section images of lithiated patterned <110> Si wafer with (a) 24hrs and (b) MD results for various crystal orientation along lateral directions. LixSi phase boundary of each case is not exactly matched but growth rates along surface are much higher than normal direction.

Figure 3-6. Surface and cross-section images of lithiated patterned <110> Si wafer with (a), (b) Cr/SiO_2 layers, (c), (d) $Cr/Cu/SiO_2$ layers.

Figure 4-5. SEM images of cracks on (110) Si wafer surface, after lithiation and delithiation. (a) (111) Si wafer surface, after lithiation. (b) Cross-sectional image of lithiated hump, and TEM image of hump. (c) Schematic of crystal structure of (111) Si wafer, along the [111] direction. (d) Random oriented cracks of (111) wafer. (e) Crack between c-Si and a-Si, after delithiation.

1. Introduction

1-1. Introduction to Li ion battery

In modern society with economic growth, energy consumption has been increased for many parts of the world. The battery is one of strong alternative way to replace non-renewable energy sources such as fossil fuels and gases accompanied with global warming [1]–[5]. Among various kind of batteries, rechargeable Li ion battery is lighter weight, compact, higher operation voltage (~ 4.0 V), specific energy (100 ~ 150 $WhKg^{-1}$) and capacity (700 ~ 2400 mAh/cell) [6]. Regarding with these advantages, Li ion battery is the most important part of hand-portable, electric transportations, entertainment, computing and telecommunication instruments necessary and widely used around us in recent [1]–[5].

Batteries including Li on battery are composed of several individual electrochemical cells connected in series or parallel for its purpose, and the electrochemical cells consists of positive, negative electrodes and electrolyte [1]. In Li ion battery, the Lithium ion and electron generation occurs through the reaction,

Cathode: $xLi \leftrightarrow xLi^{+} + xe^{-}$

Anode: $M + xLi^{+} + xe^{-} \leftrightarrow Li_xM$

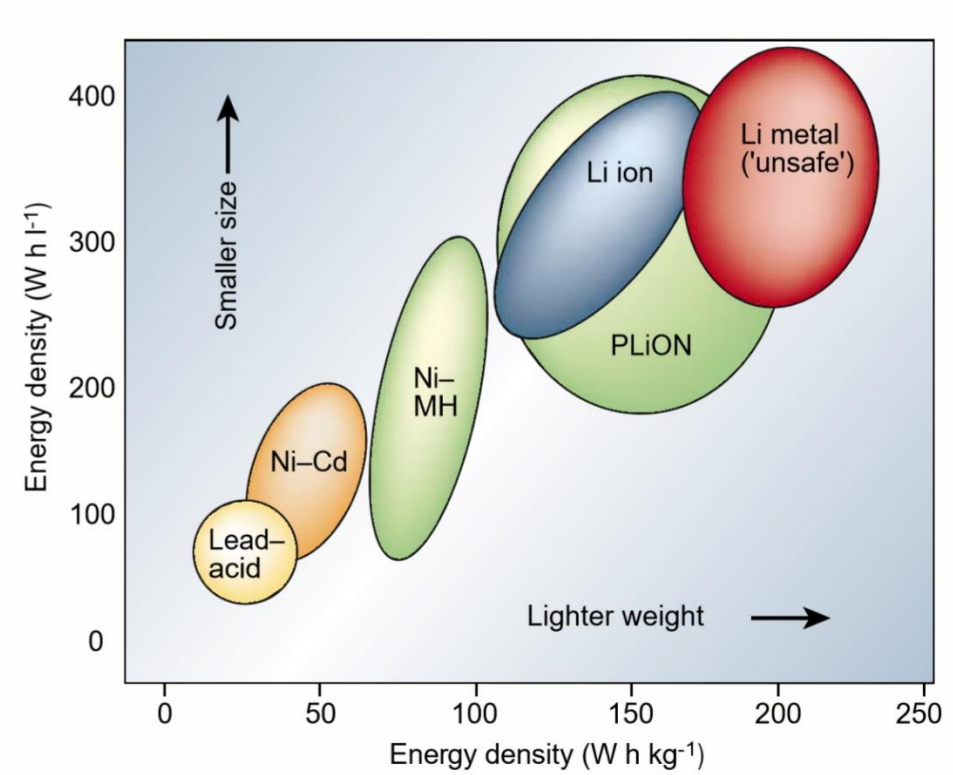

Figure 1-1. Diagram of various type of batteries. Li based battery has excellent properties of energy density.

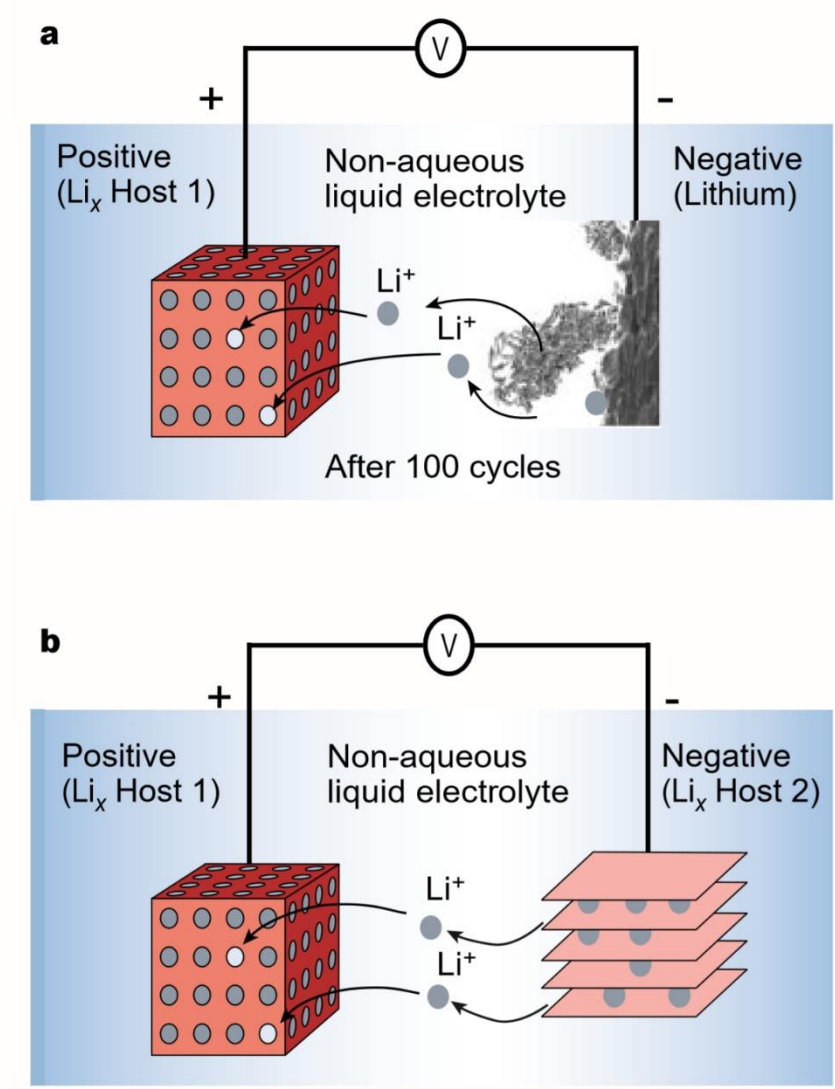

Figure 1-2. Basic component of Li ion battery; Cathode (positive), Anode (Negative) and electrolyte.

The electrons from cathode such as a lithium cobalt oxide or lithium metal move through the external circuit to current collector of anode. Then electrons combine with lithium positive ion (Li^+) and lithium atoms (Li) insert into anode material.

1-2. Anode materials for Li ion batteries

Recently commercialized anode materials and candidates for the future can be sortable into Carbonaceous, Spinel structure, metal alloys, Si-based, transition metal oxide/their composites and layered metal dichalcogenides/their composite by Roy et al [1]. In this thesis, briefly two categories are introduced; intercalation-deintercalation mechanism and phase transition mechanism materials.

1-2-1. Intercalation-Deintercalation materials

Except for phase conversion mechanism materials reacted with lithium, others can be regarded as the intercalation-deintercalation materials. Lithium atoms locate and saturate at interstitial sites however there is not loss of origin crystal structures. Carbon based materials such as Carbon nanoparticle (0-D), nanowire (1-D) [7]–[11], Graphene/Graphite (2-D) [12]–[15] and porous Carbon structures (3-D) [16]–[20] have been researched for a long time[1].

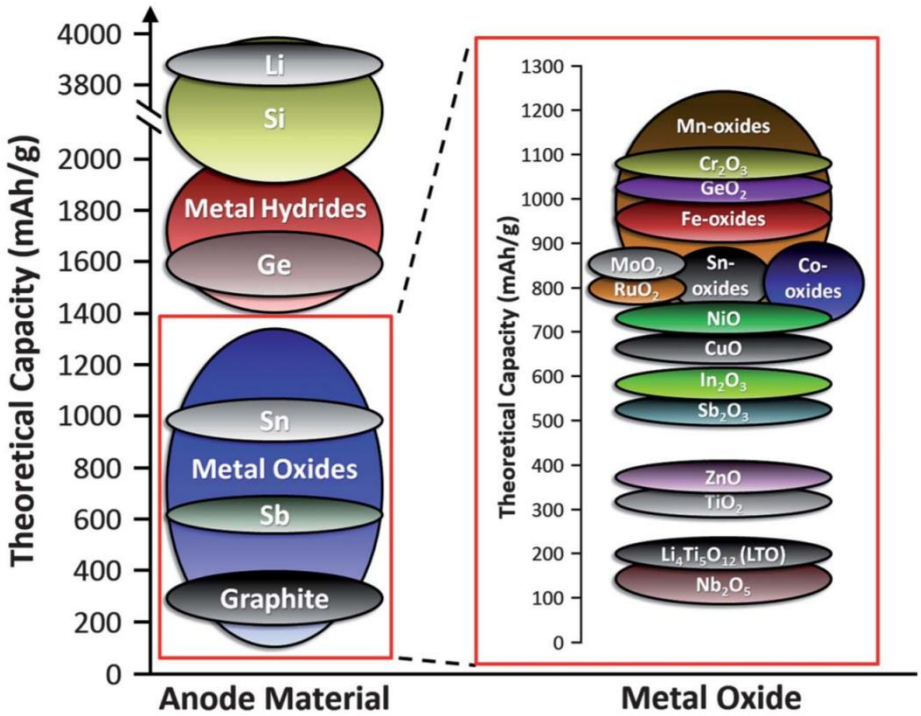

Figure 1-3. Theoretical capacity of anode candidate materials. Si is one of promising materials because of high capacity.

Graphite is well-known one of commercialized anode materials early age of rechargeable Li ion batteries. Carbonaceous anode materials also can be sortable by its crystal structures such as high crystallinity (Hard Carbon), amorphous Carbon (Soft Carbon) and cross-linked Carbon (High specific charge Carbonaceous materials) [1], [7]. However, these still have issues of significant irreversible capacity loss during first cycle even though relative theoretical capacity enhancement using nanostructures [21]. To overcome the limitations of Carbonaceous anode candidates such as lithiation potential of 0.2 V vs Li/Li^+ lithium stripping voltage especially at high current condition and insulating SEI formation [22], the Lithium titanium oxide ($Li_4Ti_5O_{12}$) of Spinel structure can be an alternative material which has higher capacity (~170 mAh/g), good cycleability and no strain or swelling during the cycles [23]. Nevertheless good characteristics, the LTO has poor electric conductivity so surface coating with good conductivity materials could be approached to cover its handicaps [24]–[26] .

1-2-2. Phase transition materials

Many kind of materials including transition metals, semiconductors and their oxides accommodate Li atoms at interstitial sites or surfaces then phase transformation or conversion occur during lithiation. Usually we can note the reaction at anode as following,

$M + xLi^+ + xe^- \leftrightarrow Li_xM$ [27], [28] (or)

$M'O + xLi^+ + xe^- \leftrightarrow Li_2O + M'$ [6], [29] (or)

$M''S_2 + 4Li + 4e^- \leftrightarrow M'' + 2Li_2S$ [30]

The M, M' and M'' can be found as (M= Si, Sn, Al, Ga, Ge, Pb, Sb), (M'= Fe, Co, Ni, Cu, Sn) and (M''= Mo, W, Ga, Nb, Ta) [12] respectively for the anode. Among those materials, the reaction of Si with Li dealt with in this thesis is correspond with the chemical formula of the first line. These candidate materials show extremely high theoretical capacity by large number of accommodation atoms but it also leads serious volume expansion up to 400%. Large swelling of materials causes high stress field and strain which can generate cracks or failure of materials.

1-3. Silicon as an anode material

In recent, Si is still a one of most promising materials for anodes in Li ion batteries (LIBs), due to its theoretical capacity of ~3500 mAh g^{-1} the largest one among candidates[2], [3], [5], [31]. Nevertheless, Si has not enough achieved to use in commercial because not fully understood and resolved problems with volume swelling and pulverization by cracks upon repeated Li insertion-extraction cause significant capacity fades as cycles continue [32]. Many efforts have been undergone to overcome these issues using nano structures, surface coatings and specific geometrical structures. In this thesis, we focused on the scale comparison between nano structures and micron structures for referring to non-uniform lithiation followed chapters.

1-3-1. Nano structures development of Si anodes

Nanomaterials have many advantages for better performance in Li ion batteries because of their small dimension. There are two significant effects; short diffusion length into entire materials and larger surface area than bigger size of materials. Thus, nanomaterials can occur the reaction cannot be taken place in micron-size materials, enforced electron transport and increase the rate of lithium insertion/extraction by following the characteristic time constant for diffusion,

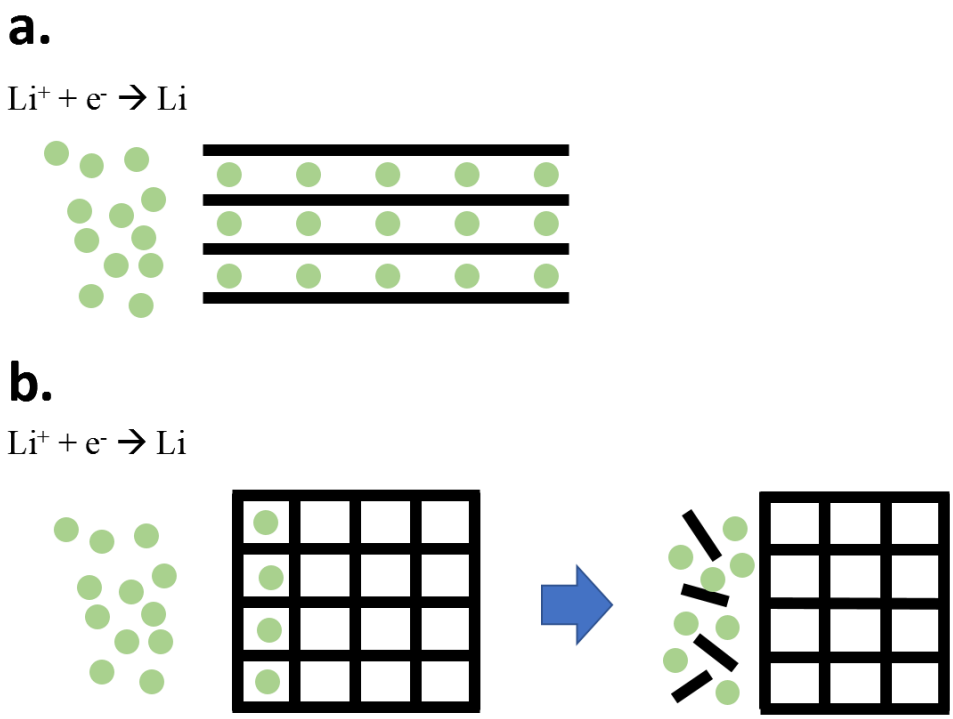

Figure 1-4. (a) Brief schematic of lithium intercalation into an anode consist of layered structure materials such as Graphite. (b) Brief schematic of lithium insertion into crystal lattice and phase transformation from crystalline to amorphous such Silicon, Germanium, Tin and so on.

$$t = L^2/D$$

where L is the diffusion length, D is diffusion coefficient respectively [5], [33]. High surface area of nanomaterials gives high contact area with electrolyte and it would increase reaction rate at whole electrodes. In addition, nanomaterials lead potential changing of electrode [34], more extensive existence for the range of composition [35]. And the strain associated with lithium insertion is better accommodated [33].

However, nanomaterials do not have only benefits for its preparation and battery's performance. More than micron or millimeters materials, nanomaterials would be hardly synthesized and controlled theirs dimensions [33]. It causes higher cost consuming than larger scale materials. Additionally, their high surface area would lead many unexpected side reaction with electrolytes and difficult to be maintained contact each other [5], [33]. Nanomaterials, especially in nanoparticles, has low tap density than larger scale ones. So volume increasing would be followed thus reducing the volumetric energy density compare with same mass of materials [5], [33]. It means that nanomaterials are not the final solution for the battery performances. Moreover, high purity of Si nano particles require high cost for huge amount of manufacture [36]. These are the reasons why the lithiation behavior in micron scale still should be studied more detail than now.

1-3-2. Lithiation behavior in nano scale crystalline Si

To clearly observe the lithiation steps including lithium intercalation into Si lattice and phase transformation from c-Si, c-Li_xSi to a-Li_xSi through the in-situ Transmission/Scanning Electron Microscope (TEM/SEM) with various type of Si nano/micro structure. The lithiated Si nanoparticle showed higher resistance to crack generation and its electrochemical properties [36]–[38]. The critical sizes which prevent crack generation are 150nm and 870nm for crystalline Si and amorphous Si respectively[38], [39]. The anodes composed by Si nano wire also show good battery performance[40], [41]. Lithiation behavior shown in Si nanowire was clearly observed by Huang et al. [42], [43]. Lithiation is taken place along the surface of nanowire and anisotropic volume expansion was observed. They suggested that small dimension of nanowire could enhance the resistance of crack forming.

During the lithiation into crystalline Si, volume expansion tends to be occurred along <110> direction. The microscopic evidences were clearly observed using nanowire, nanopillar and patterned Si wafer [43]–[45]. These results have given an important insight to analyze and forecast the lithiation behavior including mechanical analysis.

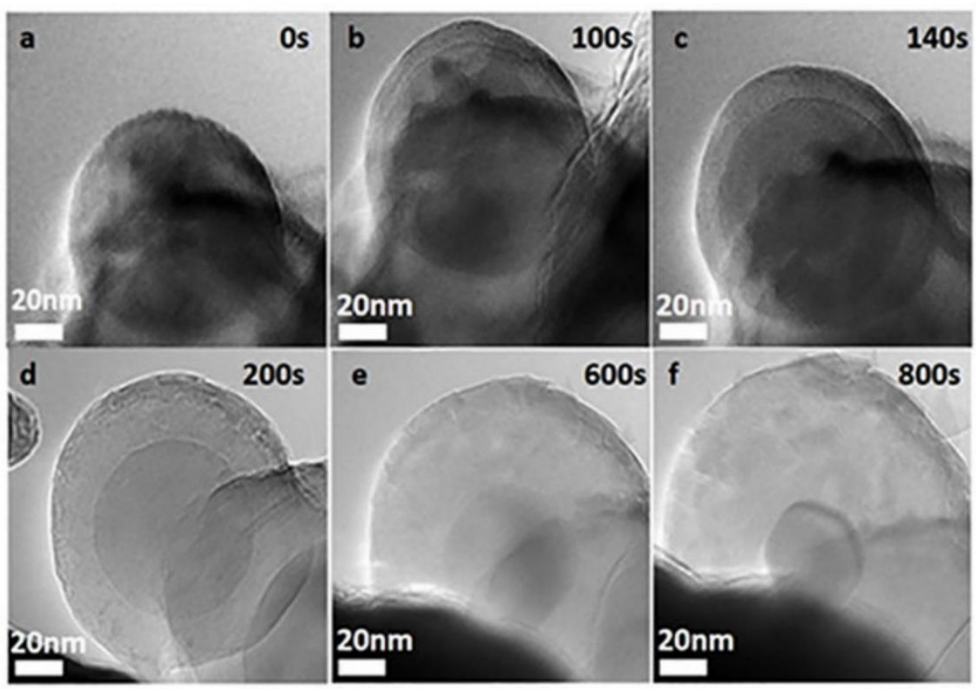

Figure 1-5. Lithiation behavior and volume expansion of nano crystalline Si. During lithiation, lithiated nano Si swells as much as 300% and forms uniform Li_xSi phase from the surface.

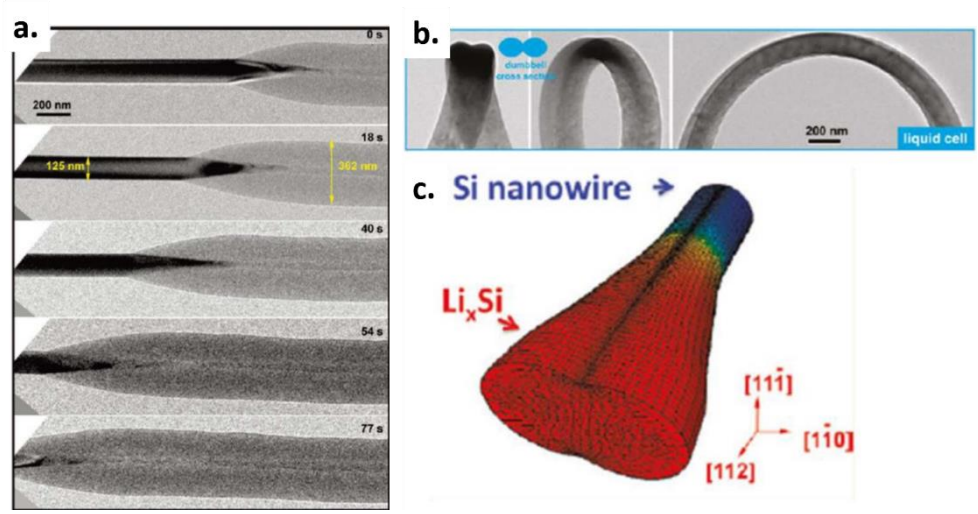

Figure 1-6. In-situ TEM results and FEM analysis for lithiated Si nanowire. Anisotropic volume expansion and LixSi phase growth were clearly observed.

1-3-3. Lithiation behavior in micro scale crystalline Si

In case of micron scale of lithiated Si particles show the distinguishable microstructure evolution during lithiation. Unlike lithiated Si nanoparticle, the core-shell structure consist of a- Li_xSi shell and c-Si core observed using in-situ TEM technique [38], [39], non-uniform and band-like lithiation were observed inside Si particles [46]. For the detail information, Choi et al. suggested using bare <100> and <110> Si wafers to find the origination of band-like lithiation [47]. In this paper, band-like lithiation is taken place only in case of lithiated <100> Si wafer with high current density condition. After delithiation at the area formed the band-like lithiation, cracks are generated and propagated much deeper inside <100> Si wafer than uniform lithiated layer [48]. However, the criteria for generating non-uniform lithiation including band-like lithiation in lithiated <100> Si wafer and its characters has not been discovered yet. These non-uniform lithiations are usually occurred in micro or larger scale Si materials. As mentioned at review of the nanomaterials, still we have many obstacles to produce massive nanomaterials. In addition, micro scale materials have benefits against several unexpected side reactions and SEI formation which can be strongly occurred in nanomaterials by its larger surface area [36]. It means that micro scale of Si also has a possibility to be a candidate of anode material in the future.

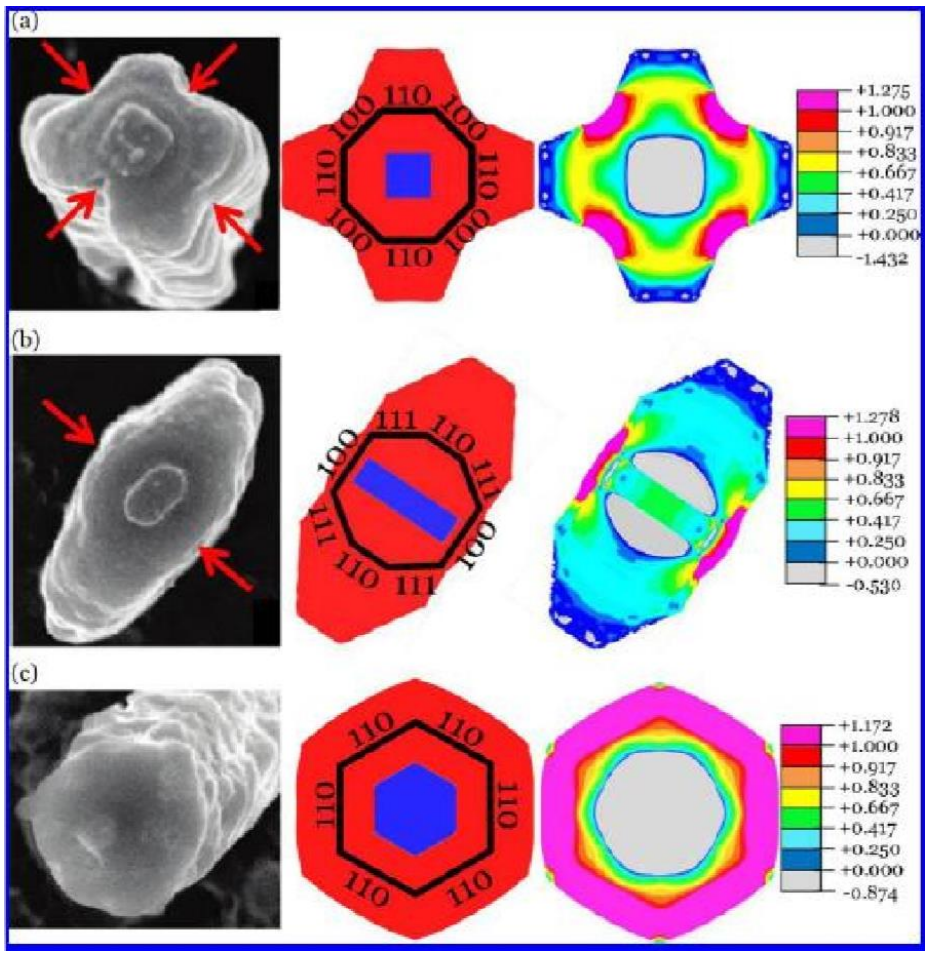

Figure 1-7. Anisotropic volume expansion of lithiated crystalline Si. It leads stress concentrated region and cracks are generated at that point.

1-4. Requirement of non-uniform lithiation and local lithium insertion

In most cases, the uniform litiation has been considered for building models and its analysis during Li insertion and phase transformation into a-Li_xSi. Indeed, several experiment results showed uniform lithiation in nanoparticles and Si wafer with Cu grid pattern [38], [42], [49]. On the other hand, non-uniform Li insertion and volume expansion has been observed at experiments using nanowires, nanopillars, micron particles and bare Si wafers [43], [44], [46]–[48]. In this thesis, the definition of uniform lithiation can be referred as a same rate of Li_xSi phase propagation which is perpendicular direction to the material surface. Directions can be normal direction of Si wafer and perpendicular of tangential plane at a contact point in case of particles or other dimensions as shown Figure 1-10. The flat phase boundaries of Li_xSi in lithiated Si wafer clearly are clearly indicated at several papers [47]–[49]. Also the good experimental result for uniform lithiation in Si particle is shown at Liu et al [38]. In many practical situations, non-uniform lithiation should be more predominant than uniform lithiation with following reasons. At first, all surface would not be contact with electrolyte. Due to components of anode electrode such as conductive carbon blacks, binders and non-uniform formation of SEI layer before Li insertion would be proceeded. These

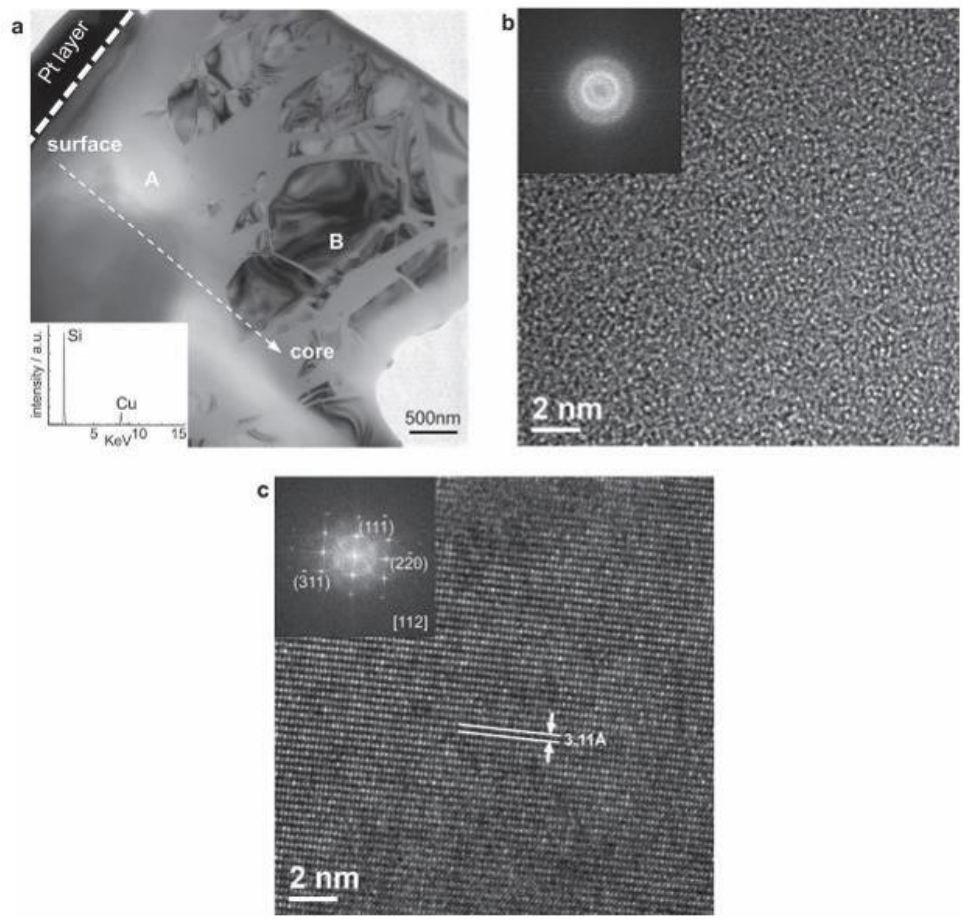

Figure 1-8. Non-uniform lithiation happens more frequently if the scale of material is bigger than a few hundred nanometers.

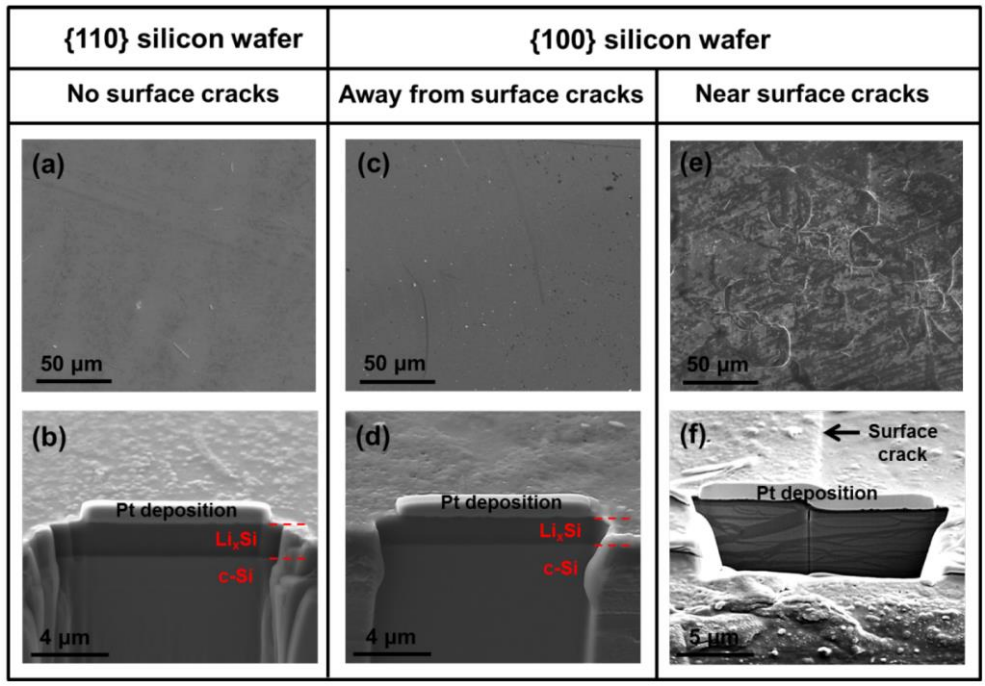

Figure 1-9. Cross-section images indicate lithiated Si layer profile at <100> and <110> Si wafer. Uniform lithiation can be taken place at <100> and <110> Si wafer both. Non-uniform lithiation was occurred only at lithiated <100> Si wafer.

materials can block Li insertion from electrolyte. In addition, electric conductivity of carbon black is much higher than SEI layer and binder usually consist of polymers. So, electrons tend to be gathered close to conductive materials. It makes differential Li concentration at the surface and amount of Li insertion into crystalline Si lattice. In case of solid-state electrolyte batteries, non-uniform lithiation will be enhanced because of their point contact between electrolyte and active materials. Size reduction of solid-state electrolyte could be a solution for it but, the probability of formation large pore and low tap density problem are still remained [33]. Also, there is a possibility which larger size particle can have two or more grains. As reported papers about anisotropic volume expansion of LixSi, they suggested and indicated experimental results that the <110> direction is the predominant diffusion sources in case of solid-state electrolyte, and (c) the possibility of multi-grain in a particle. lithiation and swelling direction than others [43]–[45], [47], [48]. Thus, the non-uniform lithiation is usual situation during lithiation process in crystalline Si. We used <100>, <110> and <111> Si wafers with pattern on them and the details will be mentioned at each chapter. Locally exposed crystalline Si can be the good experimental model to analyze the non-uniform lithiation behavior in crystalline Si-based anodes.

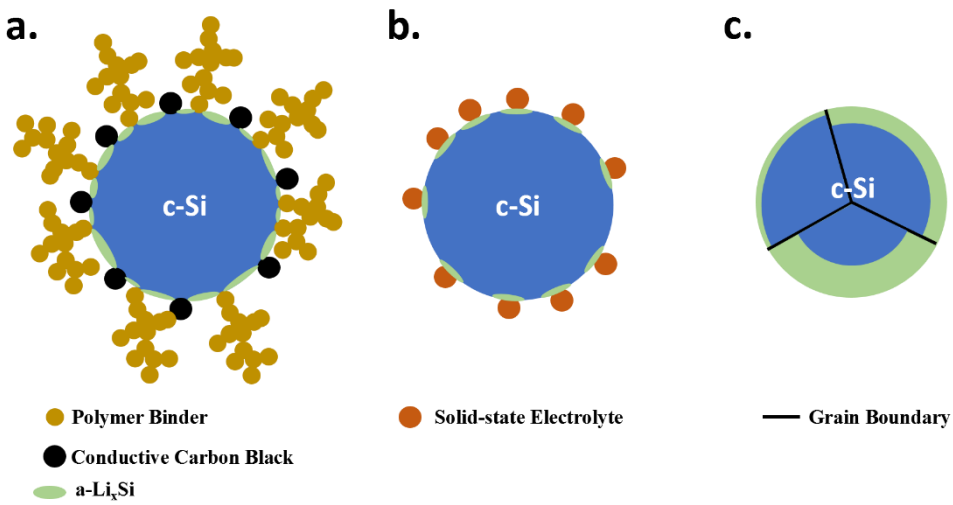

Figure 1-10. Schematics of various situation of non-uniform lithiation in practical anode consist of Si particles with over-micron size due to (a) Li diffusion blocking materials such as binder and Carbon black, (b) local Li insertion from the Li diffusion sources which is the solid-state electrolyte, (c) multigrain which has different lithiation rate.

2. Non-uniform lithiation in <100> Si

2-1. Introduction

A few number of researches using Si wafer based samples for Li ion batteries led to some important experimental findings. Goldman et al [45]. reported clear anisotropic volume expansion along the <110> direction through rectangular Si pillar or bar made by dry etching. Lee et al [44], also used nano-pillars on each orientations of Si wafer. They reported that the anisotropic volume expansion occurs preferentially at {110} surfaces. Another experimental study by Chon et al [49]. provided quantitative information on stresses associated with electrochemically induced phase transformations in crystalline (100) Si and the resulting mechanical damage. They reported the stress value at the crack formation point during delithiation, showing microscopic images where an atomically sharp interface had been introduced between a-Li_xSi layer and c-Si substrate. The microscopic observation for the crack propagation and its specific directionality affected by orientation of c-Si under Li_xSi phase was reported by Kang et al [48]. This study showed that the orientation of c-Si can determined not only lithiation and Li_xSi phase formation also crack formation and its propagation during delithiation. Because the <110> is predominant lithiation direction, mechanically anisotropic behavior is taken place by elastic modulus variation each basal direction caused by plain strain [50], [51].

In the other point of microstructure evolution during lithiation, commonly uniform flat phase boundary propagation is considered because of simplification for calculating and application for mathematical models based on assumption with uniform and homogeneous film formation. However, a few numbers of studies were suggested non-uniform lithiation behavior especially in <100> Si wafer. From the researches by Son et al. [46], and Choi et al. [47], complicated band-like (or vein-like) lithiation structure is taken place during the lithiation into micron scale Si particles and <100> Si wafer. The band-like lithiation microstructure was observed through the TEM in partially and fully lithiated Si particles by Son et al [46]. In Si wafer, Choi et al [47], suggested that the origination of band-like lithiation. Thermodynamic stability was discussed in the cases of flat phase boundary moving and formation a spherical perturbation under the flat Li_xSi phase boundary. Even though the flat phase boundary propagation is more stable than forming a perturbation, band-like structure is taken place somewhere on <100> Si wafer surface. So they suggested that some local huge volume expansion leads the micro-crack and it supplies fast Li diffusion path.

In this study, we suggest new approaches for initiation of band-like lithiation structure based on dislocation generation near battery operation temperature and its role as a fast Li diffusion path. The curvature change of lithiated <100> Si wafer was measured for understating stress evolution during non-uniform lithiation. The effect of non-uniform lithiation in aspect of stress was

discussed comparing with uniform lithiation. In addition, microscopic microstructure developments and stress evolution during its propagation with variations of current density and surface conductivity are discussed. This study can give a more detail sight to understand the failure of Si anode over micron scale and plastic deformation caused by Li solid solution or Li_xSi phase.

2-2. Experimental Procedure

Samples used as an anode electrode Si wafer with patterns were prepared by photolithography techniques. Patterns were fabricated using top-down etching and lift-off film method both but mostly lift-off was chosen. The specifications of Si wafers were 2” diameter of prime-grade, double side-polished, <100> oriented, 270 microns of thickness and 0.001 ohm-centimeter of resistivity were used. On the Si wafer, two types of film stacking were prepared with electric conductivity difference. The first type sample had 15 nm thickness of Cr film as an adhesion layer right on the Si wafer, 150 nm of Cu film was followed as a conductive layer and 150 nm of SiO_2 (E-beam deposited) film was deposited on the top of sample as a Lithium insertion barrier. On the other type sample, just Cr and SiO_2 films were deposited. The pattern is arrayed square-shape holes with 3.5 microns of edge length and 40 microns of pitch length along two <110> direction on <100> Si wafer. The c-Si was exposed to electrolyte through those patterns in shapes of square. Except for exposed region, c-Si surface is covered with $Cr/Cu/SiO_2$ or Cr/SiO_2. So, Li was intended to insert into only these exposed c-Si areas and Li insertion was certainly prevented through the cross-section observation using FIB.

For the electrochemical reaction and Multi-Beam Optical Stress Sensor (MOSS, k-Space) experiments, customized beaker cell was fabricated. Cell

body was made into PTFE which has high chemical resistance. This beaker cell has been used and described at a few researches for coupling electrochemistry and mechanics [49], [52], [53]. Li metal was used as a cathode electrode, fabricated whole 2” Si wafer for MOSS experiment and pieces of patterned Si wafer cut by 0.5” square from <100> Si wafers ware used as an anode electrode. The square-like cut Si wafer pieces were easily formed by cleavage cutting along (111) plane of <100> Si wafer. Membrane film (Cellgard) was used as a separator for minimize residue after lithiation so it can give clean surface for observing surface using Scanning Electron Microscopy (Helios 650, Nova Nanolab 200, FEI company). To improve the reliability of measurement curvature change of Si wafers and microstructure evolution, electrolyte agitation was applied. The magnetic stirrer was located at the bottom center of the cell and it can have a role as electrolyte circulation. This electrolyte agitation reduces the interface diffusion layer and supplies fresh Li ions on the sample surface [54]. It results in minimum different microstructure evolution by forming almost uniform current/potential distribution on whole planar electrodes area such as Si wafer as used these experiments. The commercial 1M $LiPF_6$ with EC or EC: DMC (1:1) were used as an electrolyte. The cells ware assembled in Ar gas filled glove box (MBraun) with low level (<0.1 ppm) of Oxygen and H_2O. Arbin BT2000 cycler was used for the lithiation at the cell.

The MOSS was used to measure the change curvature of Si wafer. Four split laser beam can measure the change of curvature along two directions vertical and horizontal. This can give us the sample bending information and indicate which type of stressed applied during lithiation. Especially for MOSS experiment, Cu grid was deposited on the <100> Si wafers and its dimension is totally same with Chon's study reported before [49]. However, higher current density was applied than that of Chon's study due to find a mechanical effect by the band-like lithiation comparing with the case of flat phase boundary moving [49].

After lithiation, the beaker cells were disassembled in glove box, and the samples were emerged into air-lock glass container which has chemical resistance with various solutions (Lock-n-Lock) filled with Dimethyl Carbonate (DMC) for preventing oxidation and hydrogenation during sample loading process between glove box and SEM. The sample loading process would take within 10 seconds. Right after opening the lid of container and samples were taken out from the DMC, they were still wet by DMC so it can be loaded in SEM without any air exposure because evaporation of DMC usually take more than 1 minute in the air, room temperature and atmosphere pressure (1 atm). The remained DMC covering the samples are fully evaporated and removed by the vacuum in the SEM chamber.

The dual-beam Focused Ion Beam (FESEM-FIB, Helios 650, FEI company) was used for observing surface and cross-section microstructure of lithiated

Si region. High current of Ga ion beam was used in order to milling rate can overcome the re-deposition rate of lithaited Si and broken pieces of samples were used in case of the large amount of lithiation sample. When the space can be occupied for scattering of ion milled particles, milling rate of lithiated Si area can be improved.

4-3. Result and Discussion

By the localized exposure c-Si region, as shown Figure 4-1, Li_xSi phase formation and its growth are shown smooth phase boundary with a little prominent right under the hole rather than perfectly flat propagation even though the flat phase boundary moving is more stable thermodynamically than phase propagation with a perturbation reported in the study by Choi et al [47]. As discussed this research, locally huge volume expansion such as a-$Li_{15}Si_4$ to c-$Li_{15}Si_4$ phase transition can lead the micro-crack due to high stress and strain energy generation. The initiation of band-like lithiation structure would be starting with expectation of stress evolution and concentration near the prominent phase boundary after high amount of Li insertion. However, even though high current density was applied to exposed c-Si region, complicated band-like structure was not formed. The 100 uA/cm^2 of current density was calculated as considered whole sample surface area so the current density can be calculated over 10 mA/cm^2 only considering exposed Si region.

This result indicates that the current density is not significant factor to form or initiating band-like lithiation. Instead of band-like lithiation microstructure evolution near the prominent phase boundary right under the exposed Si region, this can be found in the middle of holes covered by protecting films for Li insertion barrier. As shown large area cross-section image of band-like

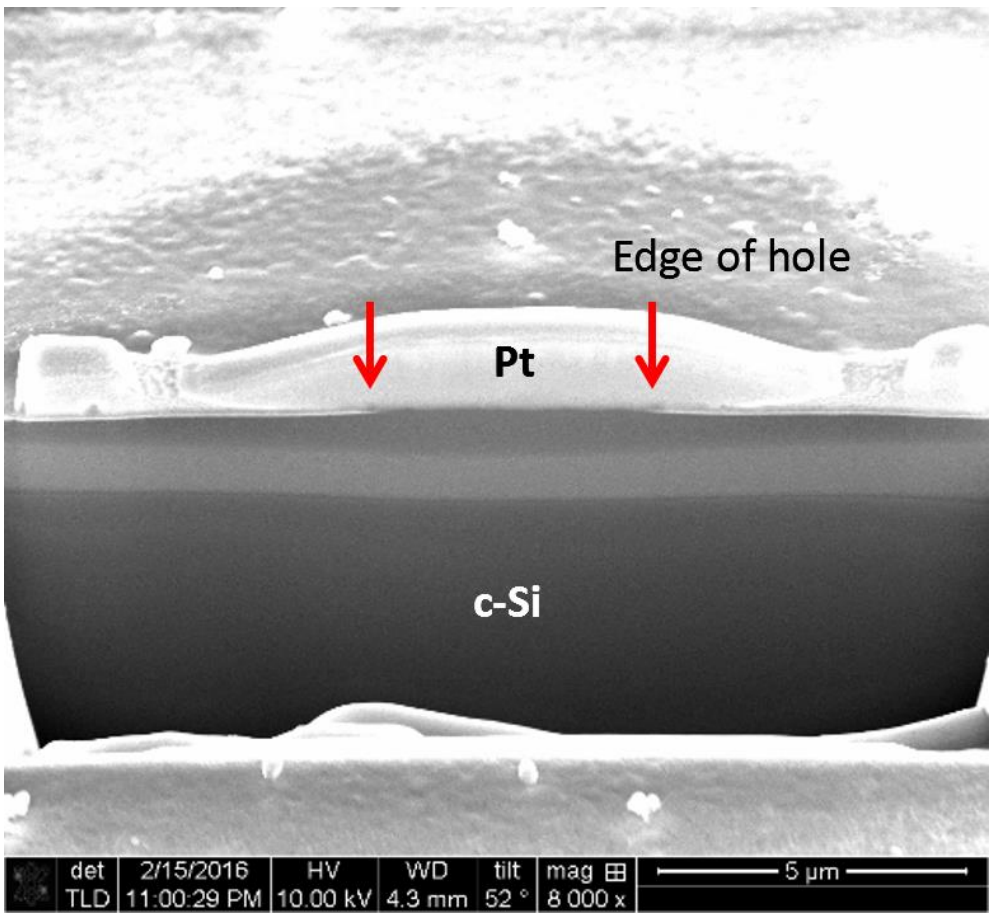

Figure 2-1. Phase boundary shape of lithiated patterned Cr/Cu/SiO_2 films on <100> Si. By localized lithiation, non-uniform lithiation and phase boundary can be formed.

lithiation microstructure area, two meaningful microstructures can be observed as shown at Figure 4-2 and 4-3. At first, non-uniform thickness of Li_xSi phase is still found similar with Figure 4-1. The thickness of Li_xSi layer is about 1.5 microns right under the holes, and the thickness at the center of two holes is about 100~200 nm or hard to be observed in SEM magnification. The second one is the band-like lithiation microstructure at the center of two holes is more complicated and has larger number of bands than one of near the holes. These two results tell us that the initiating of this complicated microstructure would start by sharp phase propagation front along lateral direction rather than normal direction of Si wafer. Also the angles between those bands and the surface, the (100) plane can be measured. Even if the (111) plane is well known the weakest plane of Si which has diamond structure makes an angle 54.7 degrees with (100) plane, mostly near the 24 degrees and parallel with the surface of bands are dominant and thicker than any other directions on (100) and (110) cross-section plane. Those bands usually showed specific angles between (100) surface but in many cases, they have a variation in range of ±5° with reported defect plane such as (111), (311). This angle offset can be explained that large volume expansion leads structural significant distortion around band-like lithiation region. However, we can figure out with some straight bands emitted and propagated from previous one and its angle measurement. In previous works dealing with dislocation in Si, not only (111) well known cleavage and dislocation glide

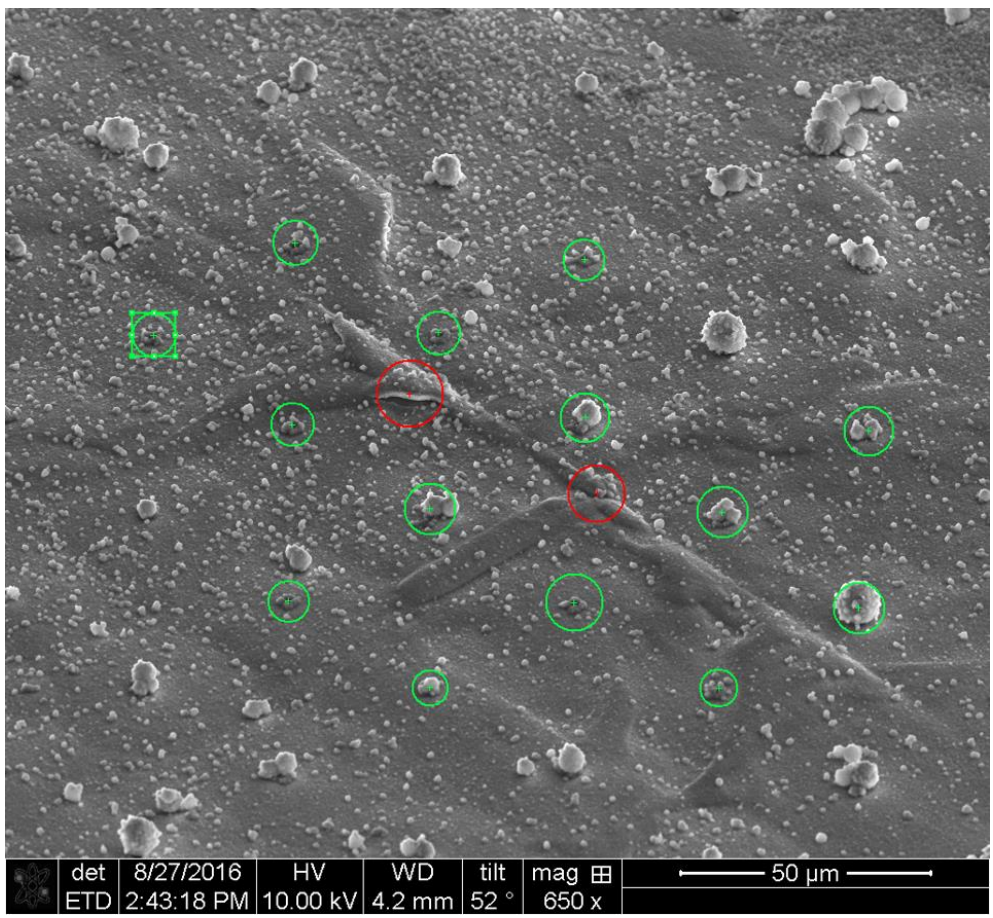

Figure 2-2. Surface image of band-like lithiation structure. The band-like lithiation structures are always accompanied with surface roughness. This is a strong evidence of plastic deformation of crystalline Si.

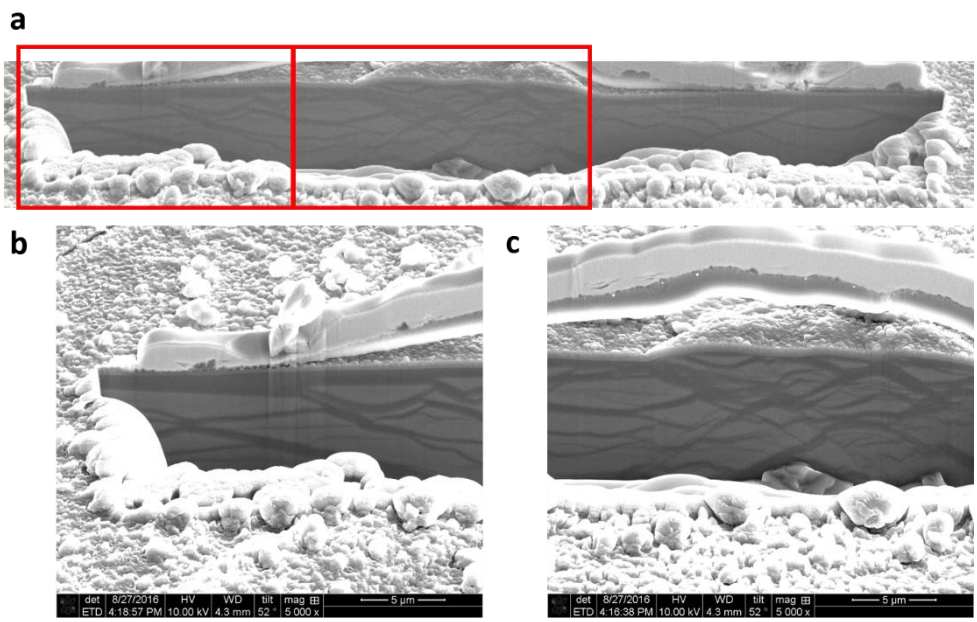

Figure 2-3. Low magnification image of the microstructure developed under surface roughened area, (b) Right under the exposed Si circle and (c) Right under the largest roughened area covered with Cr/Cu/SiO2 diffusion barrier. At (b), bands are forming more complicated structures and thickness of LixSi layer at surface is thinner than neighbor regions. Comparably, simple band-like structures are observed right under the expose Si circles and thickness of LixSi layer at surface is much thicker than (b).

plane at high temperature, (311) is also forming dislocations as the source of interstitial atoms capturing [55], [56] and the source of the loop [57]. In case of higher stress over confining pressure is applied, c-Si shows plasticity accompanied with misfit and shuffle dislocation generation and its growth even at the condition with the significantly low temperature at 77K [58]–[60]. In recent, studies about computational analysis showed the possibility of misfit and shuffle dislocations generation around the LixSi phase propagation front. By W. Zhao et al, they suggested that Li atoms diffuse along 60 misfit dislocation due to its lower energy barrier and are trapped in its core by energetically stable than other through DFT method [61].

These band-like lithiation structure observed in 2-D images captured by SEM can be defined that they are forming planes considering 3-D structure through the FIB series cross-section observation. Even though the dislocations are 1-D defects, after Li diffusion and phase transit from c-Si to a-Li_xSi along dislocations, some Li atoms can also diffuse along the <110> direction because the <110> is still the fastest Li diffusion and phase reaction rate direction. After all, it would be observed like plane.

During the lithiation and Li_xSi film growth, due to volume misfit between a-Li_xSi and c-Si, compressive stress would be applied in planar condition when the unit volume of film is higher than substrate such as Lithiated Si wafer. In previous results reported by Chon et al [49], in case of uniform flat phase boundary of Li_xSi layer on whole Si wafer surface, compressive stress

is applied regardless directions; vertical and horizontal, through Multi-beam Optical Stress Sensor (MOSS). In this case, intensity of stress can be calculated using Stoney's equation [62]. However, the situation happening development of band-like structure, a few number of its features violate the requirements of Stoney's equation; non-uniform and non-homogeneous phase growth due to gradient of Li concentration. Even though these limitation, average trend of developing stresses can be analyzed. Through the comparing difference of curvature change from the case of flat Li_xSi phase boundary moving, the effect of band-like lithiation structure evolution during Lithiation can be figured out. In observation of curvature change of c-Si substrate caused by band-like lithiation structure, unlike the case of flat Li_xSi phase boundary moving, totally lower compression is applied both two directions nevertheless higher current density condition and also their intensities are significantly different. It means that the band-like lithiation structure contributes a locally and anisotropic stress release while higher compressive stress is applied around flat Li_xSi phase boundary propagation region. Its magnitude is a little bit small so it cannot tend to break up the whole compression during Lithiation.

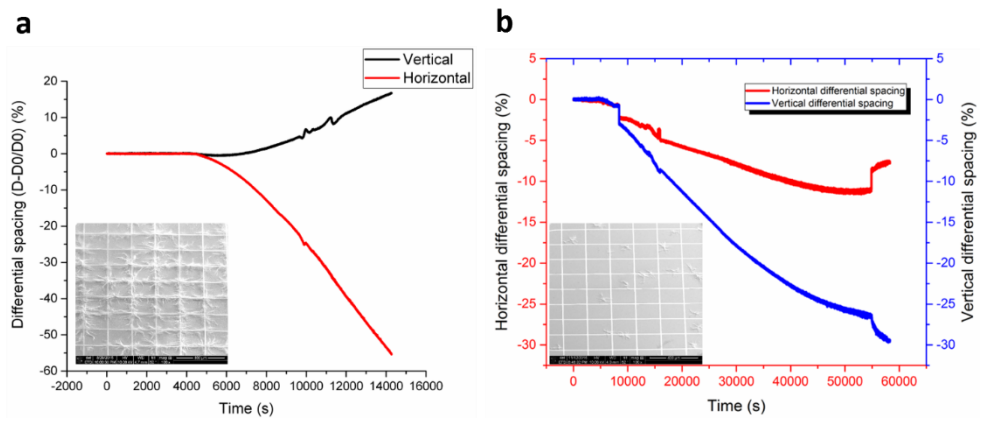

Figure 2-4. Si wafer curvature measurement during lithiation at Gu grid and Cu island pattern on <100> Si wafer. Band-like lithiation formation leads the curvature change difference. This means that band-like lithiation releases the stress during lithiation.

2-4. Conclusion

In practical lithiation into Si, band-like lithiation structure induced caused by high stress concentration neat the phase growth tip and its contribution for forming misfit dislocation was suggested. This high stress concentration is developed by huge volume expansion at phase tip so it shows phenomena similar with crack tip. The intensity of concentrated stress can be determined with current density and electrical conductivity of electrodes. Slower phase transition rate and relatively faster Li diffusion rate can lead the stress release in two Li_xSi phase growth coalescence process before large volume expansion in Low current density. In reverse, high current density condition, neighbor two Li_xSi growth and its coalescence is following after huge volume expansion. In this moment, stress and strain energy at the Li_xSi phase tip can overcome the dislocation activation energy. New generated misfit dislocations supply faster Li diffusion path than Si bulk, Li atoms can penetrate as long as 100um or longer than that depth in Si wafer. In case of Si particles, this Li_xSi phase propagation rate can result in material separation during delithiation and even in lithiation process. Also, this study suggests that Li induced dislocation development in battery operation temperature much lower than typically undergone through the thermal experimental studies for dislocation in Si. According to low temperature activated dislocations, lithiation bands can form various directions and planes having interface with c-Si. These results clearly show the reason about the failure of

Si based anode during not only delithaition and also lithiation. It is believed that this study can give an insight for further theoretical and computational model considering plasticity by dislocation.

3. Non-uniform lithiation in <110> and <111> Si

3-1. Introductions

Because of their high power, energy densities, small size and light weight lithium-ion batteries are widely used in devices which especially require portable weight and size, such as cell phones, laptops and electric vehicles [3], [4], [63]–[66]. Si is one of the strongest candidates for anode materials due to its highest theoretical capacity of ~3500 mAh/g [67]–[70]. In spite of this large capacity, lithiation into Si causes large volumetric expansion in the range of 300% to 400% [32], [70]–[72].

To understand lithiation behavior in detail, numbers of experimental and computational analysis has been reported. Several experimental investigations using Si wafers for Li ion batteries led to some important experimental findings. Goldman et al [45]. showed clear anisotropic volume expansion along the <110> direction of bulk Si wafer. Lee et al [44]. Also, used etched Si wafer with nano-pillars. They reported that the anisotropic volume expansion occurs preferentially at {110} surfaces. Another experimental study by Chon et al [49]. provided quantitative information on stresses associated with electrochemically induced phase transformations in

crystalline (100) Si and the resulting mechanical damage. They reported the stress value at the crack formation point during delithiation, showing microscopic images where an atomically sharp interface had been introduced between a-Li_xSi layer and crystalline silicon substrate.

Lots of theoretical and computational analysis of lithiation also demonstrated. Zhang et al [73] analyzed stress evolution of Si particles during lithiation and Kejie et al [74] also conducted stress analysis in the case of flat phase boundary and curved phase boundary moving in planar and spherical body. Regarding with previous reported paper, basically uniform lithiation has been assumed for their work and observed through the microscopic method. However, in the paper by Choi et al [47], vein-like lithiation microstructure development initiation is considered by micro-crack due to local volume expansion. This means that non-uniform lithiation microstructure should start from the non-uniform status of lithiation.

In this study, localized lithiation is intended for non-uniform lithiation for basal directions and planes <100>, <110>, <111>, {100}, {110} and {111} of crystalline Si. The microstructures were observed by Electron microscope and discussed about the growth rates of Li_xSi phase along the surface and normal direction of the Si wafers. Additionally, we dealt with microstructure difference dependent on surface electric conductivity and its mechanical phenomena inside and around Li_xSi phase.

3-2. Experimental procedure

To insert Li to crystalline Si locally, two-axis direction arrayed squares pattern was used shown at Fig 1b. The 2” diameter of Si wafer with p-type, <100>, <110> and <111> oriented, 0.001-0.005 ohm-cm of resistivity, 270 microns of thickness and single polished wafers were used. Patterns were made through the photolithography techniques and lift-off photoresist method was preferred than top-down method such as chemical etching or dry etching. For the Li insertion protective layer, SiO_2 film was deposited on the top of the sample and Cr film was deposited as an adhesive layer between Si wafer and Cu layer. Cu film as a conductive layer was deposited between Cr and SiO_2 film and external Cu lead was connected with conductive Cu layer. To compare with surface electric conductivity, some samples didn’t have conductive Cu layer. In this case, we used Cu foil at the bottom of Si wafer as a current collector. Only SiO_2 layer samples were also used however, due to very poor electric conductivity, lithiation was not happened. So to give a minimum conductivity Cr film were deposited at all samples. All films were deposited using E-beam deposition method. After fabrication of patterned Si wafer, samples were cut into pieces along the cleavage planes which area was 1.27 cm by 1.27 cm. They were put on the Cu foil as a current collector for no Cu layer samples but Cu foil also has a role as a Li diffusion barrier along backside of Si wafer. To reduce the electric disconnection, Ni paste was applied between Si wafer and Cu foil, and electrolyte resistive Epoxy resin

was applied at all area of side plane of Si wafer pieces. This Epoxy resin also prevent Li insertion to Si wafer at side planes. Thus, Li atom in electrolyte only can insert to top surface of Si wafer.

For the electrochemical reaction, the beaker cell was used and this beaker cell has been used for many mechanical experiments. In this experiment, large volume of beaker cell give a space to put magnetic stir bar which can agitate the electrolyte as shown at Fig 1a. Li foil was used as a cathode material and 1M $LiPF_6$ (EC: DEC 1: 1) was used as an electrolyte. The battery cycler (BT-2000, Arbin) was used for galvanostatic lithiation. As finishing lithiation, the beaker cell was disassembled and samples were delivered to SEM-FIB (Scanning Electron microscope – Focused Ion Beam, Helios 650, FEI company). To prevent air and moisture exposure, samples were taken out from the glove box (MBraun) filled with Ar gas was emerged in Dimethyl Carbornate (DMC) solution. The DMC also cleans the residual electrolyte and salts. Then, samples could be loaded into SEM-FIB chamber within a few seconds. During pumping the chamber, DMC was fully evaporated and clear sample surface could be observed.

The molecular Dynamics (MD) was undergone to find energetically stability for the lithiated microstructure and atomic position at initial lithiation step. The MD simulation used the LAMMPS open source software and Quasi-3D model to save the time, potential was calculated using the Reactive Force Field (ReaxFF) for Li vs Si. To simulate the protective film SiO_2, reflective

wall was applied and its thickness was 6 Å. Thickness of Si was 40 Å, width of system was 300 Å. The thickness of whole model was 10 Å. The energy of wall-atom interaction is given by the standard 12/6 Lennard-John Potential. Total number of atoms were 13000 ~ 15000 atoms. At first, atoms were relaxed at 1K for 25ps then heated to 1200K for 50ps. And after the temperature was hold at 1200K for 50 ~ 200ps.

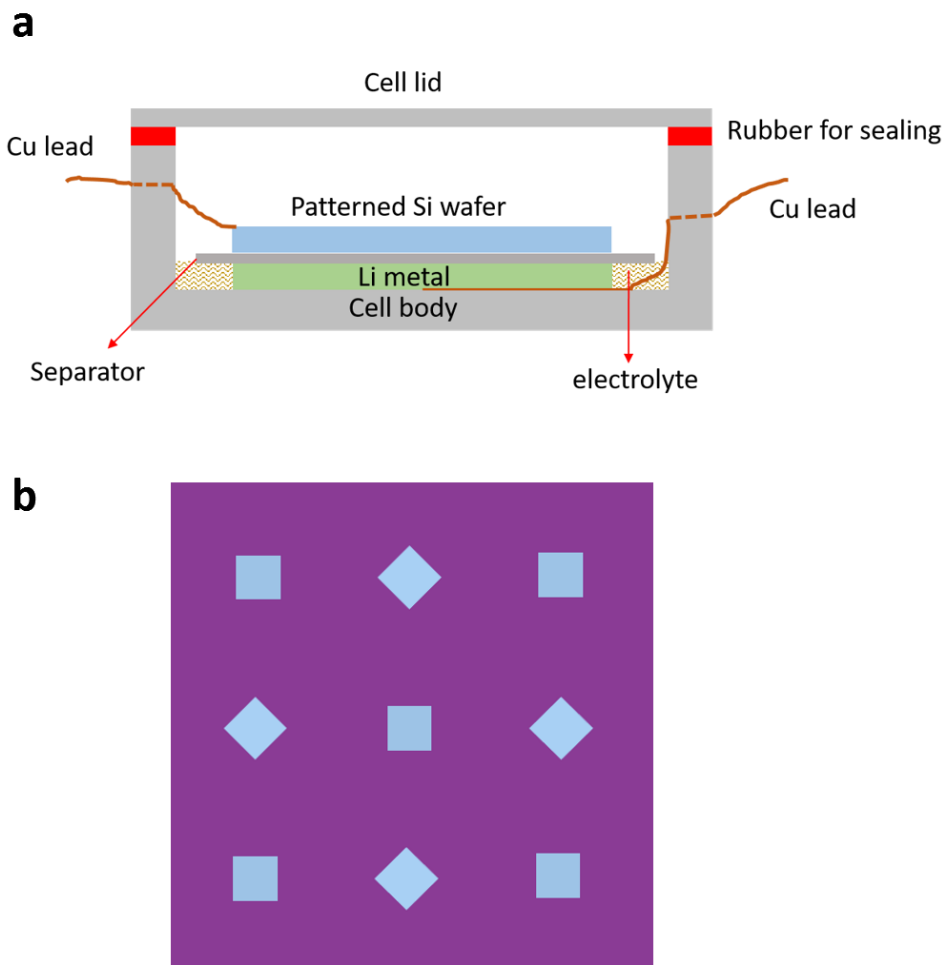

Figure 3-1. Schematics of (a) beaker cell for multi-purpose Li ion battery experiment and (b) unit cell of pattern for local Li insertion to crystalline Si.

3-3. Results and Discussion

The microstructure evolution after lithiation with 100uA/cm^2 of constant current for 24 hrs at patterned <100>, <110> and <111> were indicated at Figure 2. In these experiments, samples were loaded that its primary flat was parallel to lateral direction. Thus, the lateral direction of images for <100>, <110> and <111> would be <110>, <112> and <110> respectively. In contrast with previous reported studies [44], [45], lithiated patterned <111> Si wafer showed the largest volume expansion even though same amount of Li would be inserted. And Li_xSi phase at lithiated patterned <100> Si wafer was smallest swelling. We could understand in case of lithiated patterned <110> because the volume expansion of <110> is larger than <100> because <110> is the predominant lithiation direction. The <100> Si wafer has four <110> direction on its surface, Li_xSi phase propagation along surface can be much bigger than normal direction <100>. In <110> Si wafer, due to the normal direction is <110> so Li_xSi growth along normal direction should be larger than <100> and along surface direction growth rate was expected same with a case of <100> Si wafer. However, these results are not correspond with previous reported results which the <110> is predominant lithiation, diffusion and fastest reaction front propagation rate [44], [45], [75]. In addition, interestingly at Figure 3-2 and 3-3, these trends of lithiation and phase propagation were satisfied energetically at the Molecular Dynamics (MD) results. In situation

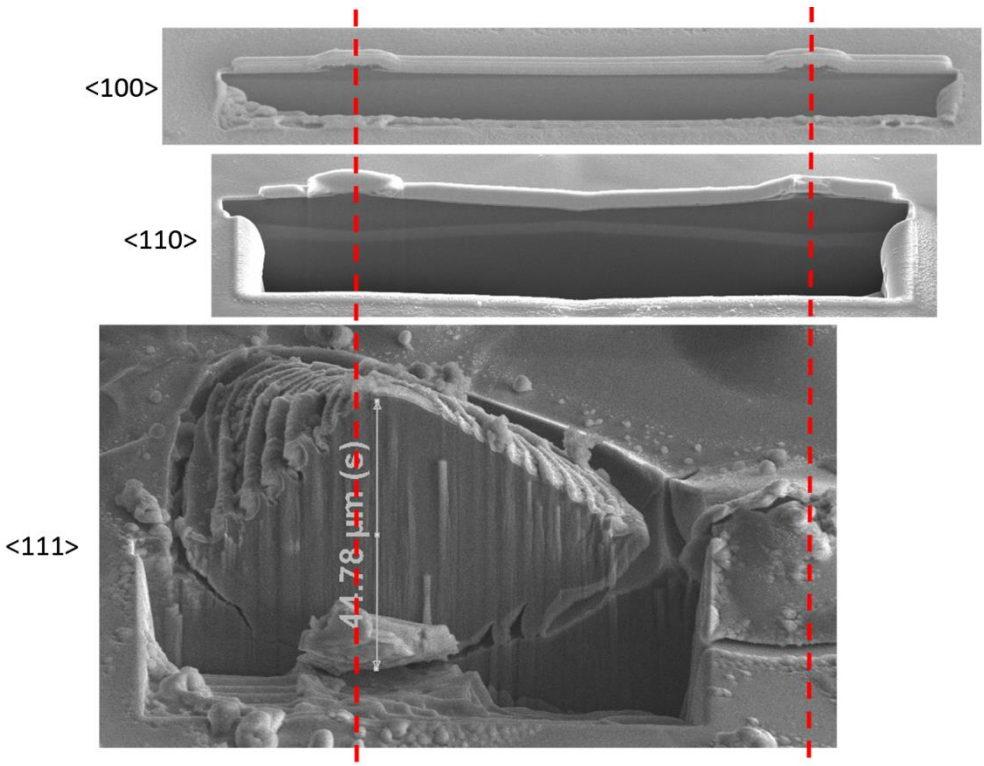

Figure 3-2. Lithiated patterned <100>, <110> and <111> Si wafer respectively. Lithiated <111> Si wafer showed the largest volume expansion. Lithiated <110> and <100> Si wafer followed magnitude of swelling in order.

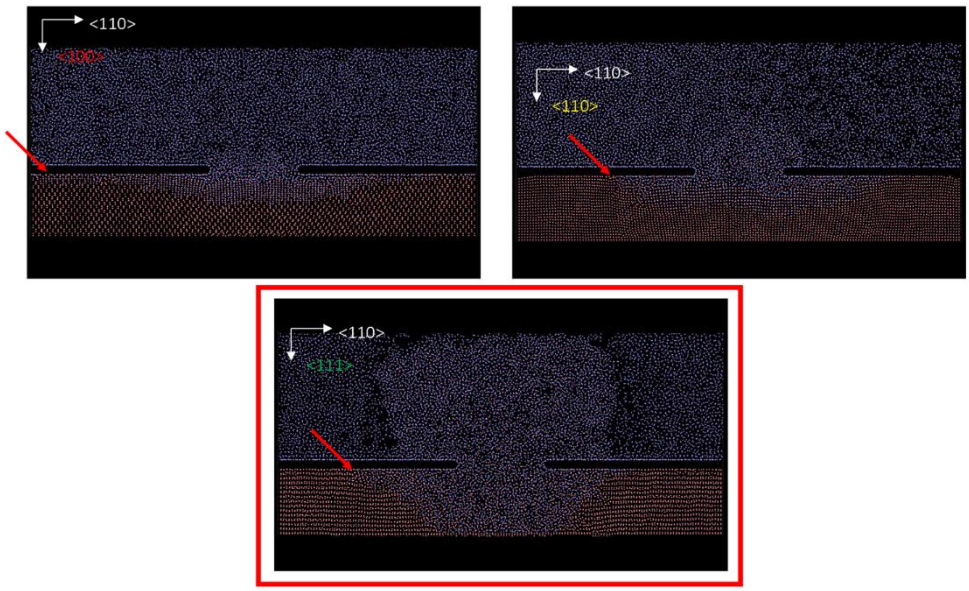

Figure 3-3. MD simulation results of local lithiation for each basal orientation of crystalline Si at initial step. MD results show a good agreement with experimental results.

of locally lithiation into crystalline Si, <111> Si wafer showed the largest lithiation. As discuss about the lithiated patterned <110> Si wafer, other lateral directions were observed using SEM-FIB. Considering the unit cell of Si diamond structure, all basal direction and plane can be observed in <110> Si wafer. As seen at Figure 4 and 5a, Li_xSi phase development for 6, 12 and 24 hrs with the lateral direction <100>, <110> and <111>. The normal direction is <110> and growth rate of Li_xSi phase propagation along the surface is same for all directions regardless its crystal orientation. And Li_xSi propagation distances for all directions are much bigger than normal direction <110> known as most lithiation and volume expansion. It means that other factor(s), not crystal orientation, can govern the lithiation behavior. For each time conditions, Li_xSi growth distances along the surface are 11 microns, 12.5 microns and over 20 microns from the center of exposed Si area respectively. Then, the Li_xSi growth rates are calculated 1.83, 1.04 and around 0.83 microns per hour. And differential growth rates at each time are 1.83, 0.25 and 0.625 microns per hour. The growth rate is the fastest at early step of lithiation and decreased after that. Then, two neighbor Li_xSi phases are getting closed, the Li_xSi growth rate would be increasing again. Comparing with lateral growth rates of Li_xSi, growth rates of normal direction are time dependent. The Li_xSi growth distances along normal direction are 0.7, 1.2 and 2.4 for 6, 12, 24hrs. To find the potential energetically satisfaction of those Li_xSi growth rates, MD simulations were done with the conditions of <110-

100>, <110-110>, <110-112> and <110-111> which note <normal direction-lateral direction>. The MD results showed that Li_xSi phase growth rate along lateral directions are much larger than normal direction in all cases. But phase boundary shapes were a little bit different each other unlike experimental results which indicated all same shape of phase boundary. The MD simulations indicated at Figure 5b, were undergone using all atoms interaction so potential or any parameters of partial or individual atom(s) could not be determined. However, the growth rate of Li_xSi phase along the surface is reliable and matched with experimental results.

Indeed, the <110> direction and {110} plane have been reported the lowest energy barrier, activation energy for diffusion and reaction front propagation rate [75], [76]. Many parameters indicate the <110> and {110} preferred properties. So, it is needed to find other parameter(s) to determine the rate of Li_xSi growth without

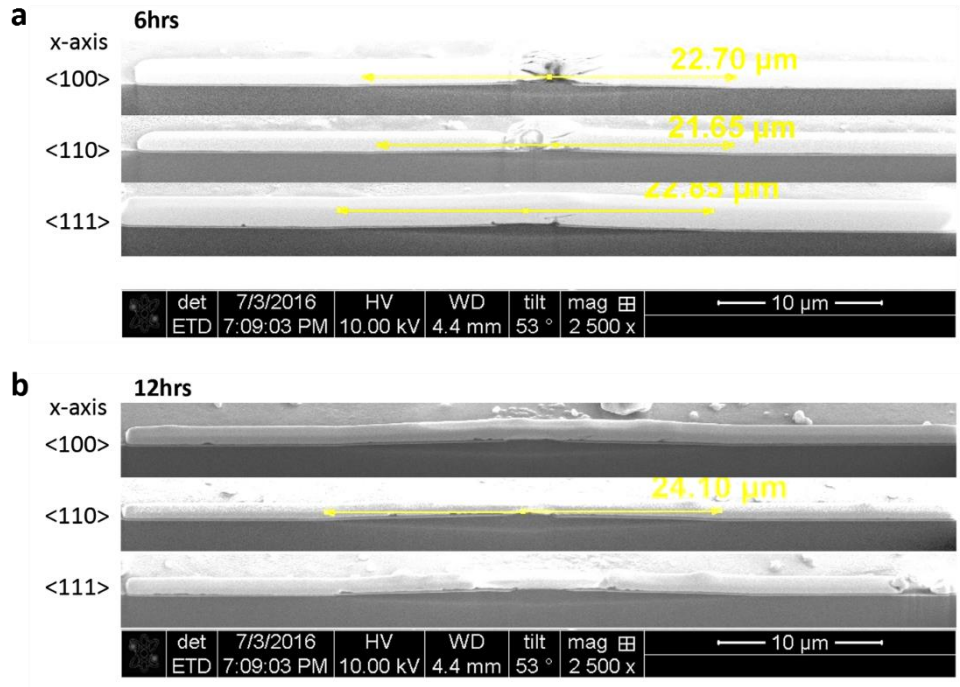

Figure 3-4. Cross-section images of lithiated patterned <110> Si wafer with various lithiation time (a) 6hrs and (b) 12hrs. During lithiation, Li_xSi phase growth rate shows same rate along all lateral directions.

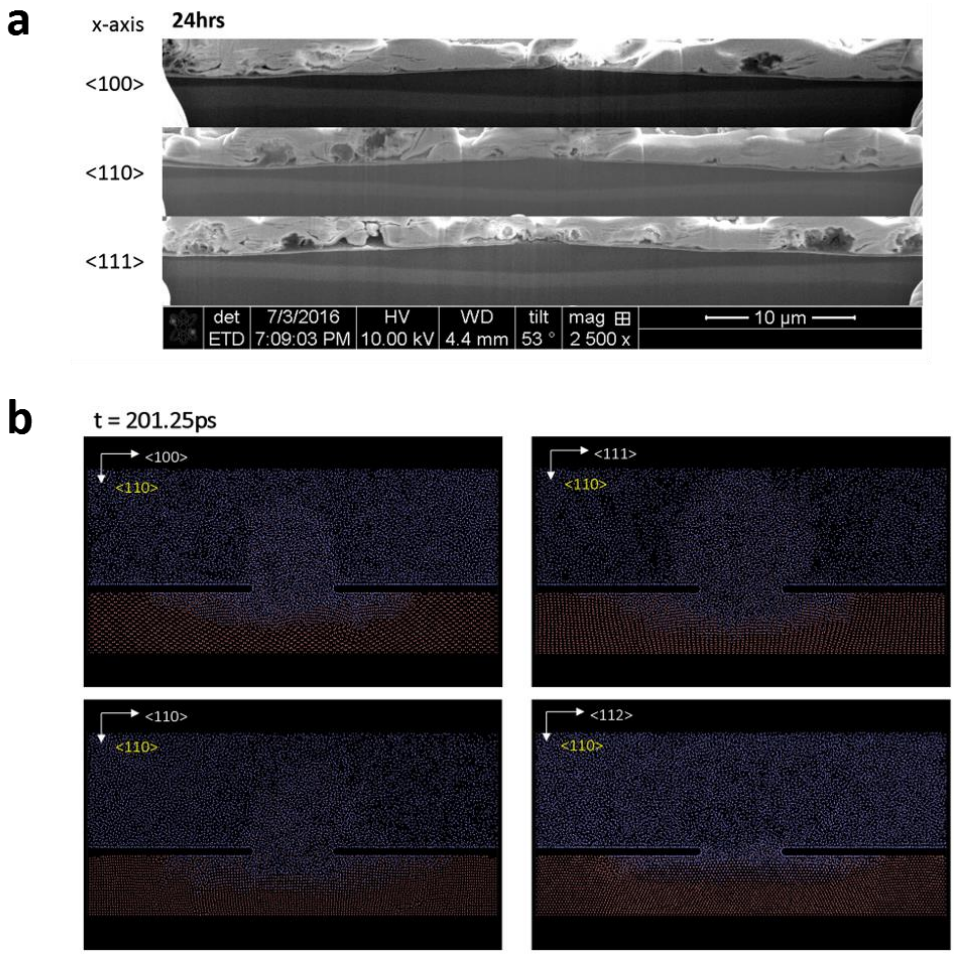

Figure 3-5. Cross-section images of lithiated patterned <110> Si wafer with (a) 24 hrs and (b) MD results for various crystal orientation along lateral directions. LixSi phase boundary of each case is not exactly matched but growth rates along surface are much higher than normal direction.

crystallography. From our another preparing researches, surface electric conductivity can govern the lithiation behavior. In addition, by Wang et al [77] reported that electron rich state enhances the amorphization of crystalline Si. According to Wang et al., the Density Functional Theory (DFT) calculation results showed that phase transformation from crystalline Si to amorphous Li_xSi was taken place much easier than other amount of electron states. Regarding those information, we prepared patterned Si wafer without conductive Cu layer between Cr film and SiO_2 protective film. As mentioned in experimental section, only SiO_2 samples were not lithiation because of very poor electric conductivity. The lack of electron on surface status wouldn't be able to make Li ions reduction to Li atoms. Thus, adhesive 15nm of Cr film was remained between protective SiO_2 film and Si substrate. In this case, the current collector should be the Cu foil at the bottom of Si substrate. After lithiation with the same condition of $100uA/cm^2$ for 24hrs with electrolyte agitation, slower Li_xSi growth rates were observed. As shown at Fig. 6a and 6b, the larger curvature of phase boundary was observed at the cross-section image of Cr/SiO_2 films on Si wafer samples. At the point of 20 microns away from the center of exposed area, center of two neighbor exposed Si area, thickness of Li_xSi phase is much more different between two samples; Cr/SiO_2 films on Si wafer and $Cr/Cu/SiO_2$ films on Si wafer. In contrast, the Li_xSi growth rates along normal direction are same for both samples. And still the Li_xSi growth rates for lateral directions were same. Unlike

crystallographic properties, the surface electric conductivity on surface can be isotropic. Indeed, the electric conductivity of Si is not isotropic. The band structure of Si lies on <100> directions. So our estimation is that actual fastest reaction front propagation rate of <110> and electron rich state enhancing amorphization of Li_xSi along <100> have interaction each other. Thus, depths of potential curve for all direction are seemed to be same such as "symmetry double-well potential or multi-well potential state". Because Li_xSi phase growth process includes kinetics and thermodynamics both.

On the other hand, when Li insert to Cr/SiO_2 films on Si wafer, by the change of LixSi shape, larger stress fields are applied. At Figure 7a and 7b, at the lithiated patterned and Cr/SiO_2 films on <110> Si wafer, cracks were observed inside the Li_xSi phase or large area of separation from the sample was observed. These results also means that Li_xSi phase boundary is getting close to hemi-sphere or has larger curvature, then higher stress can be applied at the tip of Li_xSi phase boundary than bottom area. There is another evidence from lithiated patterned and Cr/SiO_2 films on <100> Si wafer. At the cross-section images, very complicated and look like lithiation bands are formed inside the crystalline Si area. This microstructure was reported a few number of papers [46], [47] and also its origin, growth and criteria are discussed in another our paper.

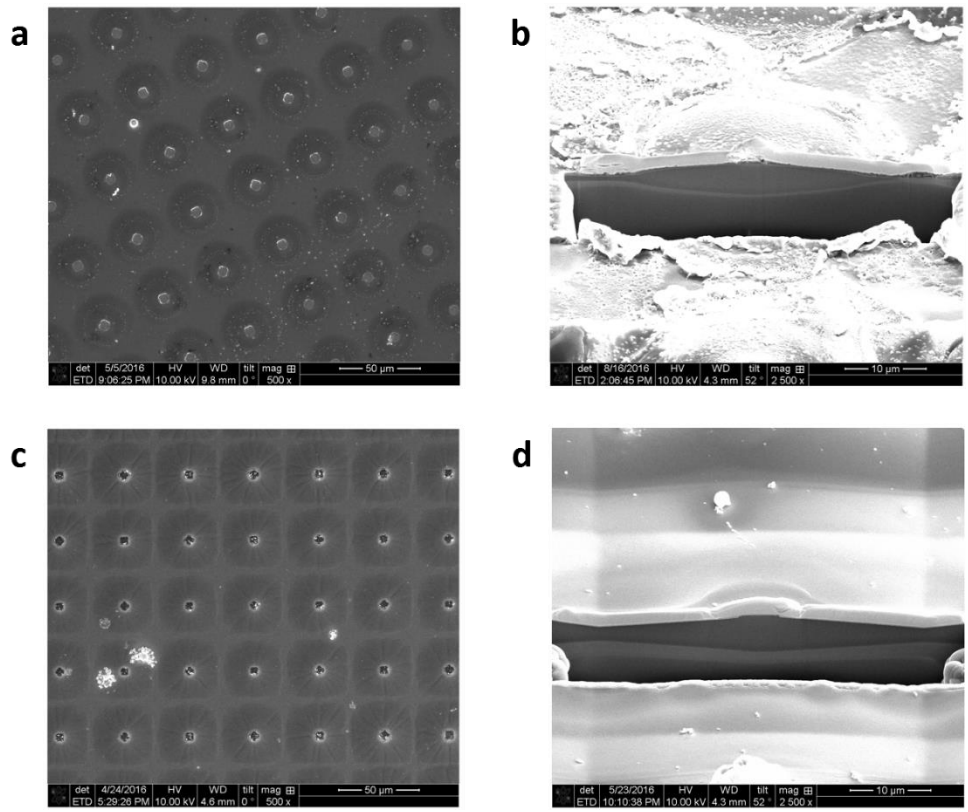

Figure 3-6. Surface and cross-section images of lithiated patterned <110> Si wafer with (a), (b) Cr/SiO_2 layers, (c), (d) Cr/Cu/SiO_2 layers.

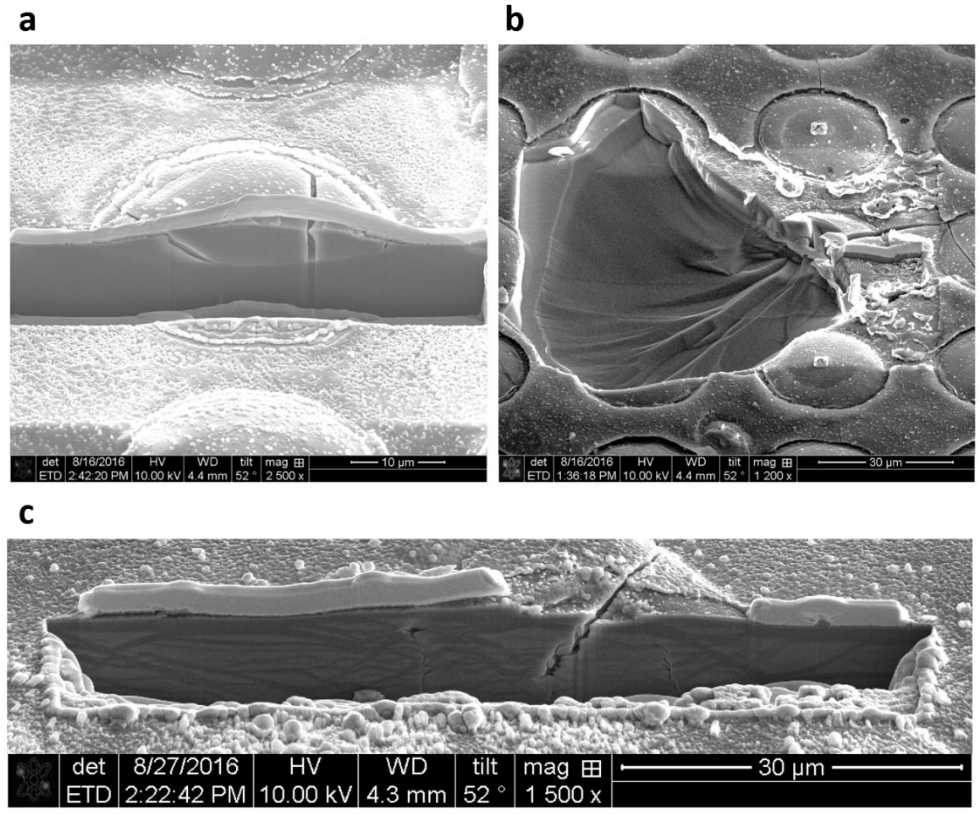

Figure 3-7. (a) Crack generation inside LixSi phase and (b) material separation from the substrate due to higher stress evolution during lithiation at Cr/SiO_2 films on patterned <110> Si wafer. And (c) band-like lithiation taken place at Cr/SiO_2 films on lithiated patterned <100> Si wafer

3-4. Conclusions

We demonstrated about the locally lithiated crystalline Si wafer for each basal orientation. Different with previous reported papers which referred the <110> directions and {110} planes are predominant lithiation orientations, when we use local exposed Si wafer, the <111> Si wafer shows the largest volume expansion and amorphous Li_xSi phase. In the lithiated patterned <110> Si wafer, unlike the open free surface structures such as nanoparticles, nanowires and nanopillars etc., the growth rates of Li_xSi phase are dependent on surface electric conductivity and isotropic along the surface directions. However, growth rate of Li_xSi along the normal direction is dependent on lithiation and phase transformation time after potential plateau region. The Molecular dynamics (MD) simulation results of atomic positions are correspond with experimental results for the local lithiation into crystalline Si. Due to the band structure along the <100> directions, which make electron rich state enhances phase transformation from crystalline Si to amorphous Li_xSi, the growth rates of Li_xSi along the surface are isotropic regardless its orientation. In same way, the growth rate of Li_xSi along can be affected by intrinsic electric conductivity and electron state so time dependent growth rate as mentioned. Because of this, we suggested the symmetry double (or multiple) well potential state for the Li_xSi growth in Si wafer.

On the other hand, electric conductivity dependent lithiation can be determine the shape of Li_xSi phase boundary. Higher curvature of phase shape can lead higher stress level at the tip of Li_xSi phase. It can make the cracks in Li_xSi phase or material separation from the parent materials.

4. Crack formation and propagation on uniform/non-uniform lithiated/delithiated crystalline Silicon

4-1. Introduction

Si is a promising material for anodes in Li ion batteries (LIBs), due to its theoretical capacity of ~3500 mAh g^{-1}. To date, this is the highest known among materials [2], [3], [5], [31]. Nevertheless, Si is not currently used commercially because problems with volume expansion, cracks, and pulverization upon repeated Li insertion-removal cause significant capacity fades as cycles continue [32].

In many cases, cracks can drive a failure of materials, and these phenomena always create new surfaces [78]–[80]. During crack formation and propagation, increased surface area can enhance the chance of SEI layer formation. Several studies revealed that the SEI layer formation on Si surface impeded Li ion transportation and caused capacity degradation of Si anode [46], [81], [82]. Cracks also cause defects among active materials which results in poor electric contact. To improve the cycle ability, these problems should be resolved in Li ion batteries with Si anode.

Several recent investigations using Si wafers for Li ion batteries led to some important experimental findings. Goldman et al [45]. showed clear anisotropic volume expansion along the <110> direction of bulk Si wafer. Lee et al [44], also used etched Si wafer with nano-pillars. They reported that the anisotropic volume expansion occurs preferentially at {110} surfaces. Another experimental study by Chon et al [49]. provided quantitative information on stresses associated with electrochemically induced phase transformations in crystalline (100) Si and the resulting mechanical damage. They reported the stress value at the crack formation point during delithiation, showing microscopic images where an atomically sharp interface had been introduced between a-Li_xSi layer and crystalline silicon substrate.

Here, we report a direct observation on the crack behavior of Si wafers with <100>, <110> and <111> axes. We introduced focused ion beam (FIB) cross-sectional analyses to observe cracks initiation and propagation in Si wafers with different orientations. The detailed three-dimensional observation of preferred crack orientation provides important insight for the design of advanced Si anode materials.

4-2. Experimental Procedure

Standard types of 2032 half-coin cells were prepared for this experiment, with Li metal foil as a counter electrode. Si wafers were cut to the size of 0.5 cm × 0.5 cm. 1 M $LiPF_6$ solution with ethylene carbonate and dimethyl carbonate (EC:DEC) was used as an electrolyte, and a constant current density of 100 μA cm^{-2} was applied for 6 hours, for both lithiation and delithiation, respectively. A detailed schematic of the coin cell is shown in Figure 4-1.

Disassembly of the coin cells was done in a glove box, filled with Ar gas. An FIB (FEI, NOVA200 dual beam system) equipped with an air-lock chamber was used for the observation of Si wafers, and TEM sample preparation. Definition of the orientation of the Si wafer was possible using the primary flat of each Si wafer. The primary flats of wafers were horizontal to the FESEM images. The air-lock system enables the observation of lithiated Si wafers without exposure to air. This air-lock system maintains an inert environment, while samples are loaded from the glove box into the FIB chamber. Details of the sample load and preparations can be found in previous research [10, 15, 16]. HRTEM (JSM-3000F, JEOL) with 300 keV was used for detailed observation of the cracks.

Crack propagation and deformation were analyzed by the following relations. It has been reported that crack formation and propagation by strain

energy release rate can be predicted by parameters with the non-dimensionalzed stress intensity factor F (α, β), and the non-dimensionalized integral of the crack opening displacement G (α, β), the so-called strain release rate [50]. Dundurs parameters (α and β) were used for obtaining the values of *F* and *G*,

$$F(\alpha,\beta,a/h)=\frac{K_I}{\sigma(\pi h)^{1/2}},\quad G(\alpha,\beta,a/h)=\frac{\int_0^a \delta(y)dy}{\pi\frac{\sigma}{E}ah} \qquad (1)$$

$$\alpha=\frac{\overline{E_1}-\overline{E_2}}{\overline{E_1}+\overline{E_2}},\ \beta=\frac{\mu_1(1-2\upsilon_2)-\mu_2(1-2\upsilon_1)}{2\mu_1(1-\upsilon_2)+2\mu_2(1-\upsilon_1)} \qquad (2)$$

where, $\bar{E}$ is the material plane strain tensile modulus defined as $E/(1-\nu^2)$, μ is the material shear modulus, K_I is the stress intensity factor, σ is the applied stress, *a* is the crack length, and *h* is the film thickness. *F* and *G* factors decide whether a crack is taking place or not, and Dundurs parameters can be invoked to explain the crack propagation direction once crack forms because these factors have elastic moduli that are dependent on the material orientation [50], [83]. Chow et al. reported that the crack propagations of soft layers on rigid crystalline Si substrate are affected by compliances of each direction of substrate

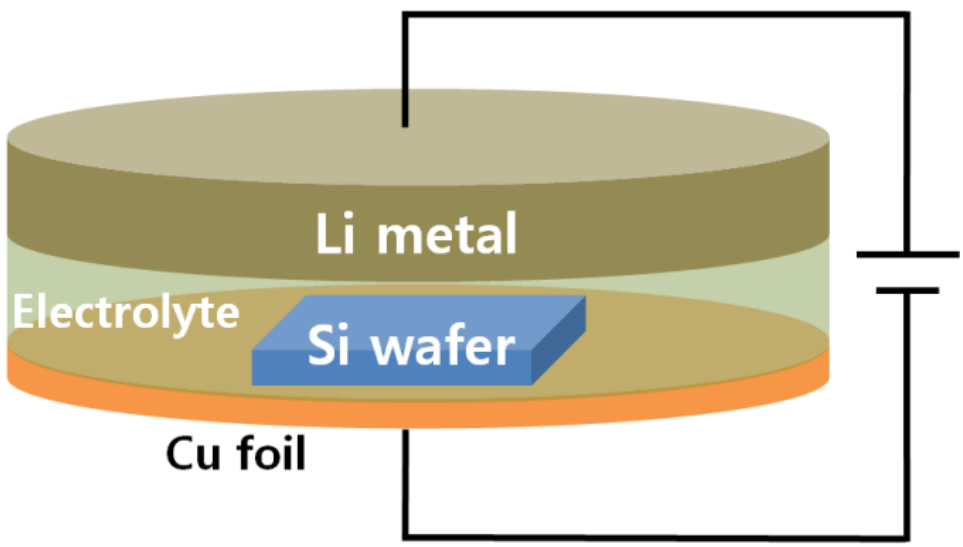

Figure 4-1. Schematic of coin cell used in this experiment.

[51]. By using a similar approach, we could analyze crack propagation observed in FESEM.

4-3. Result and Discussion

Stress generation during Li insertion and extraction is important in understanding the mechanical failure of Si anode in LIBs. A Li_xSi layer on Si wafer can be treated as a soft layer on rigid substrate (the yield strength of crystalline Si is about 7 GPa and has no plastic deformation; that of lithiated Si is less than 1 GPa, and can be plastically deformed) [14]. It has been known that compressive stress is imparted upon the Li_xSi phase at the reaction front, during Li insertion, while tensile stress is applied to the Li_xSi phase during Li extraction (Figure 4-2b) [74]. Li_xSi at the surface expands outward upon Li insertion, while the unlithiated Si inside particle constrains Li_xSi at the surface from swelling freely. This results in the unlithiated Si remaining in tensile stress, while lithiated Li_xSi at the reaction front remains in compressive stress. On the other hand, when Li is extracted, the volume of Li_xSi shrinks, and the stress status is reversed as shown in Figure 4-2c.

Figure 4-3a shows the lithiated (100) Si wafer with parallel lithiated Si layer at the reaction front. This result is consistent with previous results reported by Zhao et al [74] and Chon et al [49]. After delithiation, two different kinds of cracks were found from the

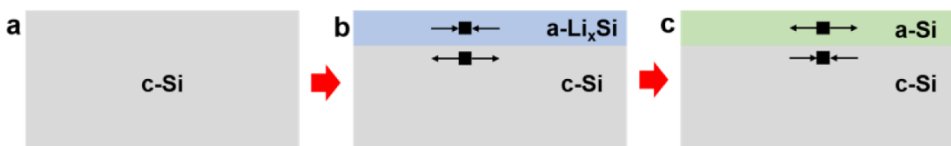

Figure 4-2. Schematics of stress field for each status of Si wafer. (a) As-made single crystal Si wafer. (b) Lithiated Si wafer; compressive stress is applied at the lithiated layer, and tensile stress is applied at the crystalline Si substrate (c) Lithiated/delithiated Si wafer; stress field is applied oppositely to the lithiated Si wafer.

delithiated (100) Si wafer surface: <110> orientated cracks and <100> oriented cracks as shown in Figure 4-3b and Figure 4-3c, respectively.

We assert that these directionalities of crack propagations in Figure 4-3b and Figure 4-3c are related to the intrinsic orientation of the Si wafer, and to the strain energy release rate G, as well. For the cracks oriented along the <110> direction in Figure 4-3b, cracks propagate the inside of the wafer, forming an angle of 54.7 degrees to the surface. This angle implies that these cracks propagate along the slip plane {111} in <110> direction inside the Si wafer. The cross-sectional image in Figure 4-3b also shows that <110> oriented cracks are initiated from the crystalline Si region. As we discussed, tensile stress is applied to the crystalline Si region during lithiation, and then tensile stress in the crystalline Si area initiates and propagates the cracks along the <110> direction on {111} planes [47].

The <100> oriented cracks shown in Figure 4-3c can be explained by the strain energy release rate G of the crack reaching the critical value of strain energy release rate G_c. In particular with the (100) Si wafer, Li_xSi layer swells upwards much smaller than <110> direction (which is sideward). So lithiated (100) Si wafer can be stated the plane strain ($\varepsilon_x \neq 0, \varepsilon_y \neq 0, \varepsilon_z = 0$). Elastic modulus in plane strain, as so-called the

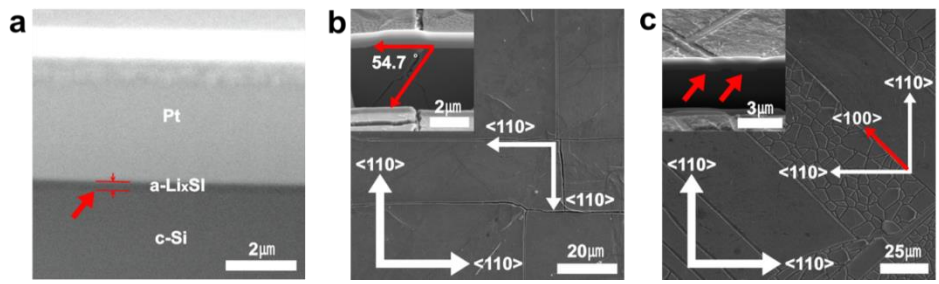

Figure 4-3. SEM images of cracks on (100) Si wafer surface after delithiation. (a) Parallel Li insertion to (100) wafer during lithiation. (b) <110> oriented cracks of (100) wafer. (c) <100> and random oriented cracks of (100) wafer.

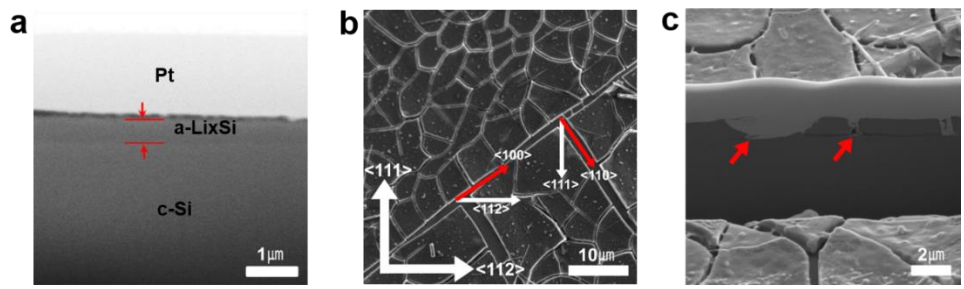

Figure 4-4. SEM images of cracks on (110) Si wafer surface, after delithiation. (a) Parallel Li insertion to (110) wafer, during lithiation. (b) <100>, <110>, and random oriented cracks of (110) wafer. (c) Interface cracks between c-Si and a-Si.

plane strain tensile modulus, was calculated and Chow et al. has reported the values of E_s (Plane strain tensile modulus of Si substrate) for each direction [51]. The E_s values of Si in <100>, <110> and <111> crystal directions are 141.2 GPa, 169.8 GPa, and 181.3 GPa, respectively [51], [84]. Upon delithiation, the Li_xSi layer at the surface becomes under tensile stress in the <100> wafer. As shown in Figure 4-3c, these <100> oriented cracks (forming an angle of 45 degree with the <110> direction) on the surface can be initiated, because the <100> direction corresponds to the lowest E_s (the most compliant direction in Si wafer). In other words, cracks can be initiated and propagated easier along <100> direction than others.

In Figure 4-4a, a cross-section of the lithiated (110) Si wafer also shows a-Li_xSi layer parallel to the Si wafer substrate. Compared with the lithiated (100) Si wafer in plane strain state, we note that the lithiated (110) wafer is simply in normal strain state. Because the <110> direction is the dominant volume expansion direction upon lithiation, the strain occurs along the 3-axes during lithium insertion into (110) Si wafer. Therefore, the calculated values of elastic moduli are different with plane strain tensile modulus ($\varepsilon_x \neq 0, \varepsilon_y \neq 0, \varepsilon_z \neq 0$). In this case, both E_{100} and E_{110} are 169 GPa and E_{111} is 181.3 GPa (higher than those (<100> and <110>) [51], [84]. Since (110) Si wafer has anisotropic mechanical properties, a directional crack can be generated based on the strain energy release rate. After lithium extraction, two different types of cracks are observed on the (110) Si wafer surface.

Figure 4b shows that the orientations of cracks on the (110) Si wafer surface are mainly in the <100> and <110> directions (forming an angle of 35.2 degree with the <112> and <111> directions, respectively). These crack propagations can also be explained by the difference in elastic modulus, being defined by compliance in the biaxial stress mode.

It is also found that cracks on the (110) Si wafer (about 800 nm of depth) propagate deeper than those on the (100) Si wafer (about 200 nm of depth). In the (110) wafer, the normal direction from the surface is <110>, which is the fastest Li diffusion direction into Si. This fast diffusion kinetics along the <110> direction is shown as thicker Li_xSi layer in (110) wafer than in (100) wafer [75]. Unlike (100) wafer, slip system induced cracks are not observed in the (110) wafer. As discussed, the <110> direction is normal to the surface in the <110> wafer, and the free volume expansion upward is favorable. Consequently, applied stress to the crystalline Si region should be less than for the case of the (100) wafer. Therefore, the applied tensile stress on crystalline (110) Si cannot reach the fracture stress of Si, but can cause the elastic deformation to crystalline Si. As a result, cracks caused by strain energy release are observed, but cracks along the slip system are not observed.

We also observed cracks at the interface between Li_xSi and crystalline Si phase in the delithiated (110) Si wafer, as shown in Figure 4-4c. This shows crack propagation along the interface between these two phases. According to studies involving detailed observation of lithiated Si, the <110> direction

of Si is the preferred direction for Li diffusion into Si, so lithiated Si can freely expand upwards in the (110) wafer [44], [45]. After delithiation, the volume of Li_xSi is reduced, and the remaining stress is relaxed, as well. Higher tensile stress can be applied between these two phases, and then the interfacial cracks can be initiated. Random direction cracks are likely caused by distributed stress, after cracks are caused by strain energy release.

In Figure 4-5a and Figure 4-5b, it is observed that irregular triangular humps are formed on the surface of the (111) wafer, after lithiation. We believe that these triangular humps are only observed in (111) wafer, because of the directionality of <110> in the <111> wafer. In the (111) wafer, there are two possible <110> directions for Li diffusion, which are {111} <110> and {100} <110>, as shown in Figure cell, and give rise to triangular shapes of Li_xSi phase in the (111) direction. (d) Random oriented cracks of (111) wafer. (e) Crack between c-Si and a-Si, after delithiation.wafer, shown in the cross-sectional image in Figure 4-5b. Once the triangular Li_xSi phase is formed, the free expansion upward is more favorable than breaking new Si bonds and diffusing inside. Therefore, lithiation-induced raised triangular humps can be formed, due to the preferred Li diffusion direction in the (111) Si wafer.

After delithiation, it is observed that cracks are initiated at the edges of humps. Random direction cracks are also formed, as shown in Figure 4-5d. No directional cracks are observed in the (111) Si wafer after delithiation,

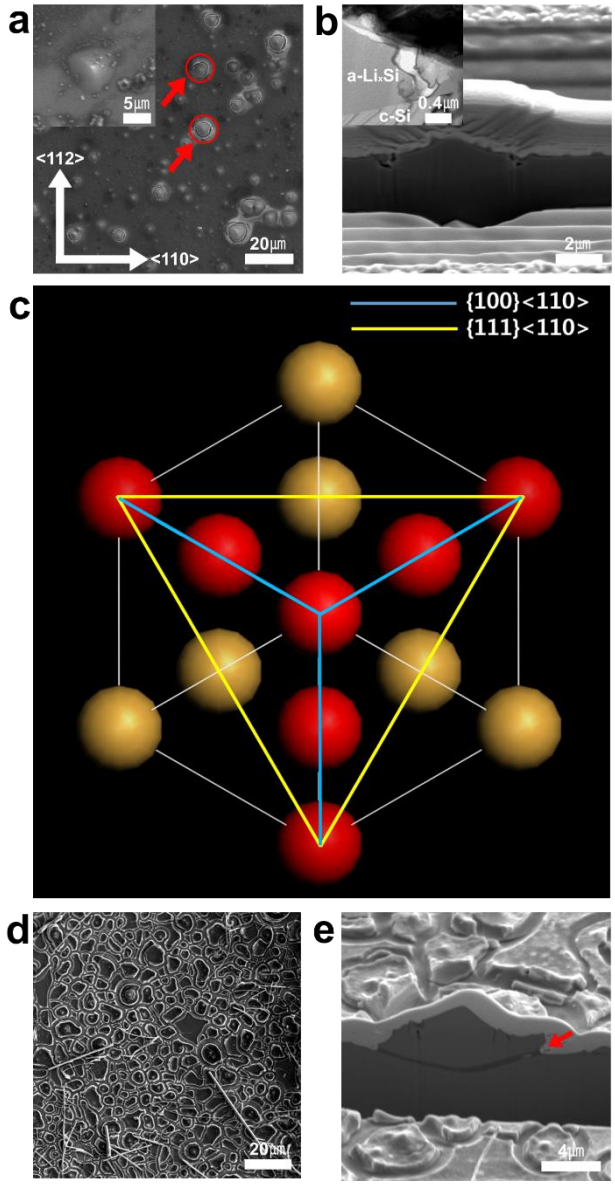

Figure 4-5. SEM images of cracks on (110) Si wafer surface, after lithiation and delithiation. (a) (111) Si wafer surface, after lithiation. (b) Cross-sectional image of lithiated hump, and TEM image of hump. (c) Schematic of crystal structure of (111) Si wafer, along the [111] 4-5c. These <110> orientations form a trigonal pyramid shape in the unit

since the {111} plane is the isotropic structure. Therefore, the strain energy release in all directions at the {111} plane is the same, and this affects the random crack initiation in the (111) Si wafer [50], [51], [83]. From the cross-sectional image of the delithiated (111) Si wafer in Figure 4-5e, cracks are observed along the interface between Li_xSi and crystalline Si. However humps still remain after delithiation, which reveals that the humps are the result of plastic deformation, induced by Li insertion into (111) Si wafer.

4-4. Conclusion

We suggest that the plane strain modulus can be used for uniform lithiation at the {100} plane, and the biaxial modulus is appropriate for the {110} plane of Si, in the case of forming a thin Li_xSi layer at the surface of the wafer. This also defines the state of soft layer on rigid substrate. In (100) Si wafer, <110> and <100> oriented cracks are observed, after lithiation/delithiation. We found that <110> cracks are initiated, and propagated along the slip system of Si; and <100> cracks occurred, because <100> is the most compliant orientation. So we can explain the Li_xSi layer formation in Si is the plane strain mode in (100) Si wafer. In (110) wafer, <100> and <110> oriented cracks are observed, after delithiation. It is known that <100> and <110> have lower elastic modulus than <111>; and this causes strong directionality of crack propagation in (110) wafer. It can be analyzed that cracks at the delithiated (110) Si wafer are dependent on just the anisotropic properties, by its crystalline orientation. (111) wafer shows different morphology changes, during lithiation. Li_xSi phase formation occurred, such as humps, and their shape is in response to the direction of volume expansion of lithiated Si. These humps are caused due to the crystallographic characteristics of (111) wafer.

5. Conclusions

In this thesis, in situation of local exposed Si wafer, the <111> Si wafer shows the largest volume expansion and amorphous Li_xSi phase. Growth rates of Li_xSi phase are dependent on surface electric conductivity and isotropic along the surface directions. However, growth rate of LixSi along the normal direction is dependent on lithiation and phase transformation time after potential plateau region. The Molecular dynamics (MD) simulation results of atomic positions are correspond with experimental results for the local lithiation into crystalline Si. Because of this, we suggested the symmetry double (or multiple) well potential state for the Li_xSi growth in Si wafer. Electric conductivity dependent lithiation can be determine the shape of Li_xSi phase boundary. Higher curvature of phase shape can lead higher stress level at the tip of Li_xSi phase. It can make the cracks in Li_xSi phase or material separation from the parent materials.

In practical lithiation into Si, band-like lithiation structure induced caused by high stress concentration neat the phase growth tip and its contribution for forming misfit dislocation was suggested. It is believed that this study can give an insight for further theoretical and computational model considering plasticity by dislocation.

We suggest that the plane strain modulus can be used for uniform lithiation at the {100} plane, and the biaxial modulus is appropriate for the {110} plane

of Si, in the case of forming a thin Li_xSi layer at the surface of the wafer. We can explain the Li_xSi layer formation in Si is the plane strain mode in (100) Si wafer. (111) wafer shows different morphology changes, during lithiation. Li_xSi phase formation occurred, such as humps, and their shape is in response to the direction of volume expansion of lithiated Si. These humps are caused due to the crystallographic characteristics of (111) wafer.

6. References

[1] P. Roy and S. K. Srivastava, “Nanostructured anode materials for lithium ion batteries,” *J. Mater. Chem. A*, vol. 3, no. 6, pp. 2454–2484, 2015.

[2] J.-M. Tarascon, “Key challenges in future Li-battery research.,” *Philos. Trans. A. Math. Phys. Eng. Sci.*, vol. 368, no. 1923, pp. 3227–41, 2010.

[3] M. Armand and J.-M. Tarascon, “Building better batteries,” *Nature*, vol. 451, no. 7179, pp. 652–657, 2008.

[4] J. M. Tarascon and M. Armand, “Issues and challenges facing rechargeable lithium batteries.,” *Nature*, vol. 414, no. 6861, pp. 359–67, 2001.

[5] A. Aricò, P. Bruce, and B. Scrosati, “Nanostructured materials for advanced energy conversion and storage devices,” *Nat. Mater.*, vol. 4, no. May, p. 366, 2005.

[6] M. V. Reddy, G. V. Subba Rao, and B. V. R. Chowdari, “Metal oxides and oxysalts as anode materials for Li ion batteries,” *Chem. Rev.*, vol. 113, no. 7, pp. 5364–5457, Jul. 2013.

[7] J. H. Trill, C. Tao, M. Winter, S. Passerini, and H. Eckert, “NMR

investigations on the lithiation and delithiation of nanosilicon-based anodes for Li-ion batteries," *J. Solid State Electrochem.*, vol. 15, no. 2, pp. 349–356, Dec. 2011.

[8] Fabing Su, Jianhuang Zeng, Xiaoying Bao, Yaoshan Yu, and Jim Yang Lee, and X. S. Zhao*, "Preparation and Characterization of Highly Ordered Graphitic Mesoporous Carbon as a Pt Catalyst Support for Direct Methanol Fuel Cells," 2005.

[9] Z. Yang, H. Q. Wu, and B. Simard, "Charge-discharge characteristics of raw acid-oxidized carbon nanotubes," *Electrochem. commun.*, vol. 4, no. 7, pp. 574–578, 2002.

[10] J. Eom, D. Kim, and H. Kwon, "Effects of ball-milling on lithium insertion into multi-walled carbon nanotubes synthesized by thermal chemical vapour deposition," *J. Power Sources*, vol. 157, no. 1, pp. 507–514, 2006.

[11] K. Evanoff *et al.*, "Towards ultrathick battery electrodes: Aligned carbon nanotube-enabled architecture," *Adv. Mater.*, vol. 24, no. 4, pp. 533–537, Jan. 2012.

[12] L. Ji, Z. Lin, M. Alcoutlabi, and X. Zhang, "Recent developments in nanostructured anode materials for rechargeable lithium-ion batteries," *Energy Environ. Sci.*, vol. 4, no. 8, p. 2682, 2011.

[13] P. Guo, H. Song, and X. Chen, “Electrochemical performance of graphene nanosheets as anode material for lithium-ion batteries,” *Electrochem. commun.*, vol. 11, no. 6, pp. 1320–1324, 2009.

[14] D. Pan *et al.*, “Li storage properties of disordered graphene nanosheets,” *Chem. Mater.*, vol. 21, no. 14, pp. 3136–3142, Jul. 2009.

[15] E. J. Yoo, J. Kim, E. Hosono, H. S. Zhou, T. Kudo, and I. Honma, “Large reversible Li storage of graphene nanosheet families for use in rechargeable lithium ion batteries,” *Nano Lett.*, vol. 8, no. 8, pp. 2277–2282, Aug. 2008.

[16] A. P. Cohn *et al.*, “Assessing the improved performance of freestanding, flexible graphene and carbon nanotube hybrid foams for lithium ion battery anodes.,” *Nanoscale*, vol. 6, no. 9, pp. 4669–75, 2014.

[17] F. Cheng, Z. Tao, J. Liang, and J. Chen, “Template-directed materials for rechargeable lithium-ion batteries,” *Chem. Mater.*, vol. 20, no. 3, pp. 667–681, Feb. 2008.

[18] H. Zhou, S. Zhu, M. Hibino, I. Honma, and M. Ichihara, “Lithium Storage in Ordered Mesoporous Carbon (CMK-3) with High Reversible Specific Energy Capacity and Good Cycling Performance,” *Adv. Mater.*, vol. 15, no. 24, pp. 2107–2111, Dec.

2003.

[19] T. Wang, X. Liu, D. Zhao, and Z. Jiang, “The unusual electrochemical characteristics of a novel three-dimensional ordered bicontinuous mesoporous carbon,” *Chem. Phys. Lett.*, vol. 389, no. 4–6, pp. 327–331, 2004.

[20] C. J. Meyers *et al.*, “Templated synthesis of carbon materials from zeolites (Y, beta, and ZSM-5) and a montmorillonite clay (K10): Physical and electrochemical characterization,” *J. Phys. Chem. B*, vol. 105, no. 11, pp. 2143–2152, 2001.

[21] J. Liu and D. Xue, “Hollow Nanostructured Anode Materials for Li-Ion Batteries,” *Nanoscale Research Letters*, vol. 5, no. 10. pp. 1525–1534, 13-Oct-2010.

[22] *Advanced Batteries*. Boston, MA: Springer US, 2009.

[23] E. Ferg, R. J. Gummow, A. Dekock, and M. M. Thackeray, “Spinel Anodes for Lithium-Ion Batteries,” *J. Electrochem. Soc.*, vol. 141, no. 11, p. L147, 1994.

[24] K. S. Park, A. Benayad, D. J. Kang, and S. G. Doo, “Nitridation-driven conductive Li4Ti5O12 for lithium ion batteries,” *J. Am. Chem. Soc.*, vol. 130, no. 45, pp. 14930–14931, Nov. 2008.

[25] H. G. Jung, J. Kim, B. Scrosati, and Y. K. Sun, “Micron-sized,

carbon-coated Li4Ti5O12 as high power anode material for advanced lithium batteries," *J. Power Sources*, vol. 196, no. 18, pp. 7763–7766, 2011.

[26] L. Zhao, Y. S. Hu, H. Li, Z. Wang, and L. Chen, "Porous Li4Ti5O12 coated with N-doped carbon from ionic liquids for Li-ion batteries," *Adv. Mater.*, vol. 23, no. 11, pp. 1385–1388, Mar. 2011.

[27] P. Limthongkul, Y. Il Jang, N. J. Dudney, and Y. M. Chiang, "Electrochemically-driven solid-state amorphization in lithium-silicon alloys and implications for lithium storage," *Acta Mater.*, vol. 51, no. 4, pp. 1103–1113, 2003.

[28] Z. Wang *et al.*, "Electron-rich driven electrochemical solid-state amorphization in Li-Si alloys," *Nano Lett.*, vol. 13, no. 9, pp. 4511–4516, 2013.

[29] J. Jiang, Y. Li, J. Liu, and X. Huang, "Building one-dimensional oxide nanostructure arrays on conductive metal substrates for lithium-ion battery anodes," *Nanoscale*, vol. 3, no. 1, pp. 45–58, 2011.

[30] M. Wang, G. Li, H. Xu, Y. Qian, and J. Yang, "Enhanced lithium storage performances of hierarchical hollow MoS 2 nanoparticles assembled from nanosheets," *ACS Appl. Mater. Interfaces*, vol. 5, no. 3, pp. 1003–1008, Feb. 2013.

[31] R. F. Service, “Solar energy. Outlook brightens for plastic solar cells.,” *Science*, vol. 332, no. 6027, p. 293, 2011.

[32] L. Y. Beaulieu, K. W. Eberman, R. L. Turner, L. J. Krause, and J. R. Dahn, “Colossal Reversible Volume Changes in Lithium Alloys,” *Electrochem. Solid-State Lett.*, vol. 4, no. 9, pp. A137–A140, 2001.

[33] P. G. Bruce, B. Scrosati, and J.-M. Tarascon, “Nanomaterials for rechargeable lithium batteries.,” *Angew. Chemie*, vol. 47, no. 16, pp. 2930–46, Apr. 2008.

[34] P. Balaya, A. J. Bhattacharyya, J. Jamnik, Y. F. Zhukovskii, E. A. Kotomin, and J. Maier, “Nano-ionics in the context of lithium batteries,” *J. Power Sources*, vol. 159, no. 1 SPEC. ISS., pp. 171–178, 2006.

[35] N. Meethong, H.-Y. S. Huang, W. C. Carter, and Y.-M. Chiang, “Size-Dependent Lithium Miscibility Gap in Nanoscale Li[sub 1−x]FePO[sub 4],” *Electrochem. Solid-State Lett.*, vol. 10, no. 5, p. A134, 2007.

[36] F. Luo *et al.*, “Review—Nano-Silicon/Carbon Composite Anode Materials Towards Practical Application for Next Generation Li-Ion Batteries,” *J. Electrochem. Soc.*, vol. 162, no. 14, pp. A2509–A2528, 2015.

[37] H. Li, X. Huang, L. Chen, Z. Wu, and Y. Liang, “A High Capacity Nano Si Composite Anode Material for Lithium Rechargeable Batteries,” *Electrochem. Solid-State Lett.*, vol. 2, no. 11, pp. 547–549, 1999.

[38] X. H. Liu, L. Zhong, S. Huang, S. X. Mao, T. Zhu, and J. Y. Huang, “Size-dependent fracture of silicon nanoparticles during lithiation,” *ACS Nano*, vol. 6, no. 2, pp. 1522–1531, 2012.

[39] L. Luo *et al.*, “Surface Coating Constraint Induced Self-Discharging of Silicon Nanoparticles as Anodes for Lithium Ion Batteries,” *Nano Lett.*, vol. 15, no. 10, pp. 7016–7022, 2015.

[40] C. K. Chan *et al.*, “High-performance lithium battery anodes using silicon nanowires.,” *Nature nanotechnology*, vol. 3, no. 1. NATURE PUBLISHING GROUP, pp. 31–5, 2008.

[41] L. F. Cui, R. Ruffo, C. K. Chan, H. Peng, and Y. Cui, “Crystalline-amorphous core-shell silicon nanowires for high capacity and high current battery electrodes,” *Nano Lett.*, vol. 9, no. 1, pp. 491–495, 2009.

[42] X. H. Liu *et al.*, “In situ TEM experiments of electrochemical lithiation and delithiation of individual nanostructures,” *Adv. Energy Mater.*, vol. 2, no. 7, pp. 722–741, 2012.

[43] X. H. Liu *et al.*, “Anisotropic swelling and fracture of silicon nanowires during lithiation,” *Nano Lett.*, vol. 11, no. 8, pp. 3312–3318, Aug. 2011.

[44] S. W. Lee *et al.*, “Fracture of Crystalline Silicon Nanopillars During Electrochemical Lithium Insertion,” *Proc. Natl. Acad. Sci. U. S. A.*, vol. 109, pp. 4080–5, 2012.

[45] J. L. Goldman, B. R. Long, A. A. Gewirth, and R. G. Nuzzo, “Strain anisotropies and self-limiting capacities in single-crystalline 3D silicon microstructures: Models for high energy density lithium-ion battery anodes,” *Adv. Funct. Mater.*, vol. 21, no. 13, pp. 2412–2422, Jul. 2011.

[46] S. B. Son *et al.*, “Microstructure study of electrochemically driven Li xSi,” *Adv. Energy Mater.*, vol. 1, no. 6, pp. 1199–1204, 2011.

[47] Y. S. Choi *et al.*, “Microstructural evolution induced by micro-cracking during fast lithiation of single-crystalline silicon,” *J. Power Sources*, vol. 265, pp. 160–165, 2014.

[48] C. S. Kang *et al.*, “Electrochemically induced and orientation dependent crack propagation in single crystal silicon,” 2014.

[49] M. J. Chon, V. a Sethuraman, a Mccormick, V. Srinivasan, and P. R. Guduru, “PHYSICAL REVIEW LETTERS 107 , 045503 2011 Real-

time Measurement of Stress and Damage Evolution During Initial Lithiation of Crystalline Silicon PHYSICAL REVIEW LETTERS 107 , 045503 2011," *Physical Review Letters*, vol. 107, no. 4. pp. 1–12, 2011.

[50] J. L. Beuth, "Cracking of thin bonded films in residual tension," *Int. J. Solids Struct.*, vol. 29, no. 13, pp. 1657–1675, 1992.

[51] L. A. Chow, Y. H. Xu, B. Dunn, K. N. Tu, and C. Chiang, "Cracking behavior of xerogel silica films on silicon substrates," *Appl. Phys. Lett.*, vol. 73, no. 20, pp. 2944–2946, 1998.

[52] V. A. Sethuraman, M. J. Chon, M. Shimshak, N. Van Winkle, and P. R. Guduru, "In situ measurement of biaxial modulus of Si anode for Li-ion batteries," *Electrochem. commun.*, vol. 12, no. 11, pp. 1614–1617, Nov. 2010.

[53] V. A. Sethuraman, N. Van Winkle, D. P. Abraham, A. F. Bower, and P. R. Guduru, "Real-time stress measurements in lithium-ion battery negative-electrodes," *J. Power Sources*, vol. 206, pp. 334–342, May 2012.

[54] J. Nikolic, E. Expósito, J. Iniesta, J. González-Garcia, and V. Montiel, "Theoretical Concepts and Applications of a Rotating Disk Electrode," *J. Chem. Educ.*, vol. 77, no. 9, p. 1191, 2000.

[55] D. J. Eaglesham, P. A. Stolk, H. J. Gossmann, and J. M. Poate, "Implantation and transient B diffusion in Si: The source of the interstitials," *Appl. Phys. Lett.*, vol. 65, no. 18, pp. 2305–2307, 1994.

[56] D. J. Eaglesham, a. Agarwal, T. E. Haynes, H.-J. Gossmann, D. C. Jacobson, and J. M. Poate, "Damage and defects from low-energy implants in Si," *Nucl. Instruments Methods Phys. Res. Sect. B Beam Interact. with Mater. Atoms*, vol. 120, no. 1–4, pp. 1–4, 1996.

[57] J. Li and K. S. Jones, "311 defects in silicon: The source of the loops," *Appl. Phys. Lett.*, vol. 73, no. 25, pp. 3748–3750, 1998.

[58] J. Rabier, M. F. Denanot, J. L. Demenet, and P. Cordier, "Plastic deformation by shuffle dislocations in silicon," *Mater. Sci. Eng. A*, vol. 387–389, no. 1–2 SPEC. ISS., pp. 124–128, 2004.

[59] J. Rabier, "High-stress plasticity and the core structures of dislocations in silicon," *Phys. Status Solidi Appl. Mater. Sci.*, vol. 204, no. 7, pp. 2248–2255, 2007.

[60] J. Rabier, L. Pizzagalli, and J. L. Demenet, *Chapter 93 Dislocations in Silicon at High Stress*, vol. 16. Elsevier, 2009.

[61] C. WANG, Q. MENG, L. YANG, and W. E. I. ZHAO, "Diffusion of Lithium in Silicon Affected By 60° Misfit-Dislocation," *Mod. Phys. Lett. B*, vol. 27, no. 23, p. 1350168, 2013.

[62] G. G. Stoney, “The Tension of Metallic Films Deposited by Electrolysis,” *Proc. R. Soc. A Math. Phys. Eng. Sci.*, vol. 82, no. 553, pp. 172–175, 1909.

[63] R. Marom, S. F. Amalraj, N. Leifer, D. Jacob, and D. Aurbach, “A review of advanced and practical lithium battery materials,” *J. Mater. Chem.*, vol. 21, no. 27, p. 9938, 2011.

[64] B. L. Ellis, K. T. Lee, and L. F. Nazar, “Positive electrode materials for Li-Ion and Li-batteries,” *Chemistry of Materials*, vol. 22, no. 3. American Chemical Society, pp. 691–714, 09-Feb-2010.

[65] S. D. Beattie, D. Larcher, M. Morcrette, B. Simon, and J.-M. Tarascon, “Si Electrodes for Li-Ion Batteries—A New Way to Look at an Old Problem,” *J. Electrochem. Soc.*, vol. 155, no. 2, p. A158, 2008.

[66] M. N. Obrovac and L. Christensen, “Structural Changes in Silicon Anodes during Lithium Insertion/Extraction,” *Electrochem. Solid-State Lett.*, vol. 7, no. 5, pp. A93–A96, 2004.

[67] W. J. Zhang, “Lithium insertion/extraction mechanism in alloy anodes for lithium-ion batteries,” *J. Power Sources*, vol. 196, no. 3, pp. 877–885, 2011.

[68] B. A. Boukamp, G. C. Lesh, and R. A. Huggins, “All-Solid Lithium

Electrodes with Mixed-Conductor Matrix," *J. Electrochem. Soc.*, vol. 128, no. 4, p. 725, 1981.

[69] Y. Wang and J. Dahn, "Comparison of the Reaction of Li[sub x]Si or Li[sub 0.81]C[sub 6] with 1 M LiPF[sub 6] EC:DEC Electrolyte at High Temperature," *Electrochem. Solid-State Lett.*, vol. 9, no. 7, p. A340, 2006.

[70] U. Kasavajjula, C. Wang, and A. J. Appleby, "Nano- and bulk-silicon-based insertion anodes for lithium-ion secondary cells," *J. Power Sources*, vol. 163, no. 2, pp. 1003–1039, 2007.

[71] M. N. Obrovac and L. J. Krause, "Reversible Cycling of Crystalline Silicon Powder," *J. Electrochem. Soc.*, vol. 154, no. 2, p. A103, 2007.

[72] S. Golmon, K. Maute, S.-H. Lee, and M. L. Dunn, "Stress generation in silicon particles during lithium insertion," *Appl. Phys. Lett.*, vol. 97, no. 3, p. 33111, Jul. 2010.

[73] Z. Jia and T. Li, "Intrinsic stress mitigation via elastic softening during two-step electrochemical lithiation of amorphous silicon," *J. Mech. Phys. Solids*, vol. 91, pp. 278–290, 2016.

[74] K. Zhao *et al.*, "Concurrent Reaction and Plasticity during Initial Lithiation of Crystalline Silicon in Lithium-Ion Batteries Lithium-ion batteries dominate the market of power sources for wireless

electronics, and are being implemented in electric vehicles," *J. Electrochem. Soc.*, vol. 159, no. 3, pp. 238–243, Jan. 2012.

[75] M. Pharr, K. Zhao, X. Wang, Z. Suo, and J. J. Vlassak, "Kinetics of Initial Lithiation of Crystalline Silicon Electrodes of Lithium-Ion Batteries," *Nano Lett.*, vol. 12, no. 9, pp. 5039–5047, Sep. 2012.

[76] W. Wan, Q. Zhang, Y. Cui, and E. Wang, "First Principles Study of Lithium Insertion in Bulk Silicon," *J. physics. Condens. matter*, vol. 22, p. 415501, 2010.

[77] Z. Wang *et al.*, "Electron-rich driven electrochemical solid-state amorphization in Li-Si alloys," *Nano Lett.*, vol. 13, no. 9, pp. 4511–4516, Sep. 2013.

[78] A. Hellemans, "Cracks: More than just a clean break," *Science (80-.).*, vol. 281, no. 5379, pp. 943–944, 1998.

[79] C. Guerra, J. Scheibert, D. Bonamy, and D. Dalmas, "Understanding fast macroscale fracture from microcrack post mortem patterns.," *Proc. Natl. Acad. Sci. U. S. A.*, vol. 109, no. 2, pp. 390–4, Jan. 2012.

[80] A. Livne, E. Bouchbinder, I. Svetlizky, and J. Fineberg, "The near-tip fields of fast cracks.," *Science*, vol. 327, no. 5971, pp. 1359–1363, 2010.

[81] J. Graetz, C. C. Ahn, R. Yazami, and B. Fultz, "Highly reversible

lithium storage in nanostructured silicon," *Electrochem. Solid State Lett.*, vol. 6, no. 9, pp. A194–A197, 2003.

[82] H. Wu *et al.*, "Stable cycling of double-walled silicon nanotube battery anodes through solid–electrolyte interphase control," *Nat. Nanotechnol.*, vol. 7, no. 5, pp. 310–315, Mar. 2012.

[83] T. Ye, Z. Suo, and A. G. Evans, "Thin film cracking and the roles of substrate and interface," *Int. J. Solids Struct.*, vol. 29, no. 21, pp. 2639–2648, 1992.

[84] J. J. Wortman and R. A. Evans, "Young's Modulus, Shear Modulus, and Poisson's Ratio in Silicon and Germanium," *J. Appl. Phys.*, vol. 36, no. 1, pp. 153–156, Jan. 1965.

Abstracts (in Korean)

최근 리튬 이온 전지는 높은 전력과 에너지 밀도, 그리고 가벼운 무게로 인해 모바일 장치, 전기자동차 및 많은 장비들의 보조 전력 장치로서 널리 사용되고 있다. 긴 수명과 장치의 성능 향상을 위해 양극과 음극에 큰 용량의 재료가 요구된다. 실리콘은 대체후보물질 중 가장 큰 이론 용량을 (3500mAh/g)을 가지고 있는 강력한 후보 물질 중 하나이다. 그러나 지난 수십년간 음극재료로서 실리콘에 대해 열역학적, 이동현상적, 기계적 거동에 대해 많은 연구가 수행되었으나 여전히 완전한 이해가 되지 않았다

이 논문에서는 실리콘의 기저방향들에서 비등방성 리튬화실리콘상의 성장에 대해 연구이다. 많은 연구들에서, <110> 방향과 {110} 면은 리튬화가 지배적으로 일어나는 방향과 면으로 잘 알려져 있다. 다양한 나노기둥, 나노와이어, 나노입자와 같은 나노구조를 이용한 비등방성 리튬화와 팽창, 균열 발생이 명확하게 제시하고 있다. 이렇게 자유표면을 가진 구조들과 비교하여, 실리콘 웨이퍼에 국소적으로 실리콘 영역을 노출시키는 패턴을 만들어 실험에 이용하였다. 전도성 금속과 절연성 박막을 이용하여 국소적 리튬화를 만들어냈다. 자유표면을 가진 구조들과는 다르게 실리콘 웨이퍼 내부에서는

표면방향으로는 결정학적 방향과 관계없이 등방성 상의 성장을 보여주었다. {110} 웨이퍼를 사용한 경우에도 {110}면이나 <110>방향은 지배적인 리튬화 현상을 보여주지 않았다. 리튬화 실리콘의 상 성장속도를 결정하는 요소가 무엇인지 구조적으로, 혹은 그 외적 방법으로 논의되었다. 또한 표면전기전도성과 리튬화 실리콘의 성장과의 관계에 대해서도 서술되었다.

첫번째 장에서는 <100> 웨이퍼에서 리튬화시 발생하는 주목할 만한 미세구조인 “띠형상 리튬화 구조”에 대해 논의되었다. 국소적 리튬화 실험을 통해 띠형상 리튬화 구조의 기원과 조건을 밝혀냈다. 실리콘은 공유결합을 하고 있는 취성이 강한 재료로 알려져있다. 그러나 최소 두개 이상의 이웃한 두 리튬화 실리콘 사이에서 전위의 발달 가능성을 확인하였다. 전에 보고된 많은 논문들에서 실리콘의 소성변형과 전위 형성, 고리, 이동에 대해서 언급되었듯이, 리튬이 실리콘에 들어감으로써 소성변형이 일어날 수 있는 환경을 만들어 줄 수 있음을 제시하였다. 그리고 투과전자현미경분석을 통해 리튬화 띠에 대한 결정학적 분석도 동반되었다.

두번째 장에서는 실리콘의 기저방향들에서 비등방성 리튬화실리콘 상의 성장에 대해 연구이다. 많은 연구들에서, <110> 방향과 {110} 면은 리튬화가 지배적으로 일어나는 방향과 면으로 잘 알려져 있다. 다양한

나노기둥, 나노와이어, 나노입자와 같은 나노구조를 이용한 비등방성 리튬화와 팽창, 균열 발생이 명확하게 제시하고 있다. 이렇게 자유표면을 가진 구조들과 비교하여, 실리콘 웨이퍼에 국소적으로 실리콘 영역을 노출시키는 패턴을 만들어 실험에 이용하였다. 전도성 금속과 절연성 박막을 이용하여 국소적 리튬화를 만들어냈다. 자유표면을 가진 구조들과는 다르게 실리콘 웨이퍼 내부에서는 표면방향으로는 결정학적 방향과 관계없이 등방성 상의 성장을 보여주었다. {110} 웨이퍼를 사용한 경우에도 {110}면이나 <110>방향은 지배적인 리튬화 현상을 보여주지 않았다. 리튬화 실리콘의 상 성장속도를 결정하는 요소가 무엇인지 구조적으로, 혹은 그 외적 방법으로 논의되었다. 또한 표면전기전도성과 리튬화 실리콘의 성장과의 관계에 대해서도 서술되었다.

세번째 장에서는 실리콘 웨이퍼에 리튬화, 탈리튬화시 발생하는 균열과 그 전파에 대해서 직접적으로 관찰하였다. 다른 세 <100>, <110>, <111> 실리콘 웨이퍼에서 발생하는 균열을 분석하였다. 리튬화 시 서로 다른 결정학적 방향과 변형에너지가 다르기 때문에 그들은 서로 유사하지 않다. 특히 <111> 웨이퍼에서는 삼각형 형태의 둔턱을 형성함을 처음으로 관찰하였다. 실리콘의 리튬화 시 부피팽창, 균열, 분쇄 등이 상업화하는데 큰 화두임을 고려할 때, 이 연구는 향상된

실리콘 기반 음극을 개발하는 데 있어 중요한 시각을 제공할 것으로 기대된다.

핵심어: 리튬이온전지, 리튬화 실리콘, 핵생성과 성장, 확산, 미세구조, 비등방성 상 성장, 균열 전파

학번: 2011-20617

강 찬 순